The Plant Cell, Vol. 23: 304–321, January 2011, www.plantcell.org © 2011 American Society of Plant Biologists

ATP Synthase Repression in Tobacco Restricts Photosynthetic Electron Transport, CO_2 Assimilation, and Plant Growth by Overacidification of the Thylakoid Lumen [OA]

Markus Rott,[a,1] Nádia F. Martins,[a,1] Wolfram Thiele,[a] Wolfgang Lein,[a] Ralph Bock,[a] David M. Kramer,[b] and Mark A. Schöttler[a,2]

[a] Max-Planck-Institut für Molekulare Pflanzenphysiologie, D-14476 Potsdam-Golm, Germany
[b] Michigan State University–Department of Energy Plant Research Laboratory and Department of Biochemistry and Molecular Biology, Michigan State University, East Lansing, Michigan 48824

Tobacco (*Nicotiana tabacum*) plants strictly adjust the contents of both ATP synthase and cytochrome b_6f complex to the metabolic demand for ATP and NADPH. While the cytochrome b_6f complex catalyzes the rate-limiting step of photosynthetic electron flux and thereby controls assimilation, the functional significance of the ATP synthase adjustment is unknown. Here, we reduced ATP synthase accumulation by an antisense approach directed against the essential nuclear-encoded γ-subunit (*AtpC*) and by the introduction of point mutations into the translation initiation codon of the plastid-encoded *atpB* gene (encoding the essential β-subunit) via chloroplast transformation. Both strategies yielded transformants with ATP synthase contents ranging from 100 to <10% of wild-type levels. While the accumulation of the components of the linear electron transport chain was largely unaltered, linear electron flux was strongly inhibited due to decreased rates of plastoquinol reoxidation at the cytochrome b_6f complex (photosynthetic control). Also, nonphotochemical quenching was triggered at very low light intensities, strongly reducing the quantum efficiency of CO_2 fixation. We show evidence that this is due to an increased steady state proton motive force, resulting in strong lumen overacidification, which in turn represses photosynthesis due to photosynthetic control and dissipation of excitation energy in the antenna bed.

INTRODUCTION

The capacity of the photosynthetic light reactions to provide ATP and NADPH must be closely adjusted to their metabolic consumption by the Calvin cycle, the subsequent reactions of dark metabolism such as starch synthesis, and other anabolic pathways within the chloroplast. Upon hyperactivity of the light reactions, the metabolic regeneration of $NADP^+$, ADP, and P_i will limit photosynthetic electron transport, resulting in detrimental side reactions. $NADP^+$ limitation would result in electron transfer to alternative acceptors, such as O_2, generating reactive oxygen species. These can damage the photosynthetic apparatus itself and also initiate cell death responses (Kim et al., 2008).

Reduced ADP and P_i regeneration results in substrate limitation of the thylakoid ATP synthase, reducing proton efflux from the lumen and resulting in an increase of the proton motive force (pmf) across the thylakoid membrane (Takizawa et al., 2008; Kiirats et al., 2009). Under standard growth conditions, the pmf is partitioned into an electrochemical component ($\Delta\Psi$) and a proton gradient (ΔpH) in such a way that the pH value of the thylakoid lumen is usually kept between 7.0 and 6.5 (Takizawa et al., 2007). However, in response to short-term imbalances between proton translocation into the lumen by photosynthetic electron transport and use of the pmf for ATP synthesis, the pH of the thylakoid lumen can drop below 6.5. This initiates photoprotective feedback responses such as nonphotochemical quenching (qN), which is the thermal dissipation of excess excitation energy in the photosystem II (PSII) antenna bed in the form of heat (Szabó et al., 2005). This is achieved through protonation of the PsbS antenna protein and by activation of the violaxanthin deepoxidase, which converts the xanthophyll violaxanthin into zeaxanthin. Also, plastoquinol (PQ) reoxidation at the cytochrome b_6f complex (cyt-bf) is slowed down when the lumenal pH falls below 6.5, thereby restricting linear electron flux (reviewed in Kramer et al., 1999). This mechanism is called photosynthetic control.

Although both protective mechanisms become active at pH values below 6.5, they are fully activated only at a lumenal pH below 6.0, with the cyt-bf response peaking at slightly lower pH values than qN (Takizawa et al., 2007). In case of a severe imbalance between light reactions and dark metabolism, a more pronounced overacidification of the thylakoid lumen can result in damage to plastocyanin (PC) and disintegration of the oxygen-evolving complex of PSII (Krieger and Weis, 1993; Kramer et al., 1999). However, these types of damage were so far only studied in vitro (Kramer et al., 1999). It is still a matter of debate whether or not these highly acidic pH values in the lumen can be established in vivo or whether they are efficiently avoided by

[1] These authors contributed equally to this work.
[2] Address correspondence to schoettler@mpimp-golm.mpg.de.
The author responsible for distribution of materials integral to the findings presented in this article in accordance with the policy described in the Instructions for Authors (www.plantcell.org) is: Mark A. Schöttler (schoettler@mpimp-golm.mpg.de).
[OA]Open Access articles can be viewed online without a subscription.
www.plantcell.org/cgi/doi/10.1105/tpc.110.079111

downregulation of linear electron flux by qN and decreased PQ reoxidation rates. Also, it is still questionable whether plants can control the lumenal pH by altering the relative pmf partitioning into $\Delta\Psi$ and ΔpH. Under nonstressed conditions, the pmf partitioning can be highly variable between different plant species (Takizawa et al., 2007). Therefore, a variable partitioning of pmf could conceivably enable plants to regulate the onset of photoprotective mechanisms and avoid photodamage by overacidification.

While the short-term responses of plants to an imbalance between light reactions and dark metabolism are well understood, much less is known about the long-term adjustment of photosynthetic electron transport and the proton circuit to a reduced metabolic demand. Long-term changes in assimilation capacity are known to occur during leaf ontogenesis, when assimilation declines with leaf age (Schöttler et al., 2004, 2007a), but also in response to several environmental stresses, such as drought stress (Tezara et al., 1999). Also, light intensities during growth strongly alter leaf assimilation capacity. Under the majority of these conditions, photosystem I (PSI) contents are constant (Anderson et al., 1988; Bailey et al., 2001; Schöttler et al., 2004). Also, PSII contents do not change much, except upon changes in growth light intensity (Bailey et al., 2001). Good indications exist that the capacity of linear electron flux is predominantly controlled by cyt-bf contents, which are highly variable and closely correlated with assimilation capacity (Evans, 1988; Anderson, 1992). This observation is in line with cyt-bf catalyzing the rate-limiting reaction step of linear electron transport, PQ reoxidation (Hope, 2000; Kirchhoff et al., 2000). Indeed, a strong contribution of cyt-bf to photosynthetic flux control has been shown by antisense repression of its essential Rieske Fe_2-S_2–containing subunit (Price et al., 1995, 1998). PC content was also shown to correlate with photosynthetic flux rates (Burkey, 1993, 1994; Schöttler et al., 2004).

Finally, substantial changes in ATP synthase contents in response to changes in light intensity (Anderson et al., 1988; Evans, 1988), leaf age (Schöttler et al., 2007a), and drought stress (Tezara et al., 1999; Kohzuma et al., 2009) have been reported, and these also parallel assimilation capacities. However, the functional significance of the adjustments of ATP synthase content has remained unclear, especially because other components of the photosynthetic apparatus (in particular, cyt-bf) show parallel changes under most of these conditions, possibly suggesting a coregulation.

To determine the contribution of the ATP synthase to photosynthetic flux control, we specifically repressed the ATP synthase content in tobacco (*Nicotiana tabacum*) using two independent approaches. First, we repressed the *AtpC* gene encoding the essential γ-subunit with an antisense approach. In *Chlamydomonas reinhardtii*, it has been shown that AtpC availability controls the biogenesis of the ATP synthase complex (Drapier et al., 2007). Downregulation by an antisense strategy was appropriate because an *Arabidopsis thaliana atpC* T-DNA insertion line suffered from destabilization of the entire complex and degradation of the other ATP synthase subunits, so that photophosphorylation was entirely abolished (Bosco et al., 2004). In addition, we repressed the translation initiation efficiency of the essential chloroplast-encoded β-subunit, encoded by the *atpB* gene, which forms part of the catalytic center of the extrinsic CF_1 subcomplex of the ATP synthase.

We report here the generation of transgenic and transplastomic tobacco lines that contain ATP synthase contents from 100% to <10% of wild-type levels. Physiological analysis of lines with greatly reduced ATP synthase revealed a strongly increased pmf across the thylakoid membrane, leading to the activation of photoprotective mechanisms and downregulation of linear electron flux already in low light. This resulted in repressed leaf assimilation and plant growth, supporting a central role of the ATP synthase in regulating photosynthesis. Additionally, the analysis of these mutants enabled the identification of regulated steps of ATP synthase biogenesis in higher plants.

RESULTS

Generation of *AtpC* Antisense Lines and Functional Organization of Their Photosynthetic Apparatus

The *AtpC* antisense plants were obtained from a large collection of antisense lines generated from a tobacco leaf cDNA library (Lein et al., 2008). The tobacco *AtpC* antisense construct was generated from an EST covering a 601-bp-long fragment of the *AtpC* gene (spanning positions 760 to 1361 of the coding region). This region is unique to *AtpC*. Searches of the *AtpC* EST against all known tobacco ESTs (in the National Center for Biotechnology Information [NCBI]), the complete *Arabidopsis* genome (in NCBI and The Institute for Genomic Research [TIGR]), and all Solanaceae species (in TIGR) did not reveal any sequence stretches with more than 18 bp homology. Therefore, off-target effects of the chosen antisense sequence are unlikely to occur. However, as the tobacco genome is not yet fully sequenced, they cannot be entirely excluded (see Discussion).

Transformation of tobacco plants with the antisense construct yielded several transgenic lines, two of which were characterized in detail. Whereas one line displayed a strong growth retardation (line atpC1), the other showed only a mild growth phenotype (line atpC2; Figure 1A). Flowering of the atpC2 mutant was delayed on average by 3 to 4 d, while flowering of the atpC1 mutant was delayed by several weeks in comparison to the wild type. In general, the strength of the growth phenotypes was somewhat variable between individual progeny plants. This is typical of antisense transformants because the underlying epigenetic effect is reset in meiosis (Kooter et al., 1999).

Transcript accumulation was analyzed by RNA gel blot analysis and revealed a much stronger repression of the *AtpC* transcript abundance in line atpC1, in agreement with the growth phenotypes (Figure 1B). To analyze adaptive responses of the photosynthetic apparatus to the *AtpC* antisense repression, we determined several physiological parameters using the youngest fully expanded leaf of plants at the onset of flowering, usually leaf number six or seven from the top. We measured leaf absorptance and chlorophyll content, chlorophyll *a*/*b* ratio, assimilation and respiration capacities, the quantum efficiency of CO_2 assimilation, maximum quantum efficiency of PSII, and photosynthetic complex contents (Table 1). While chlorophyll content, chlorophyll *a*/*b* ratio, and leaf absorptance were comparable in

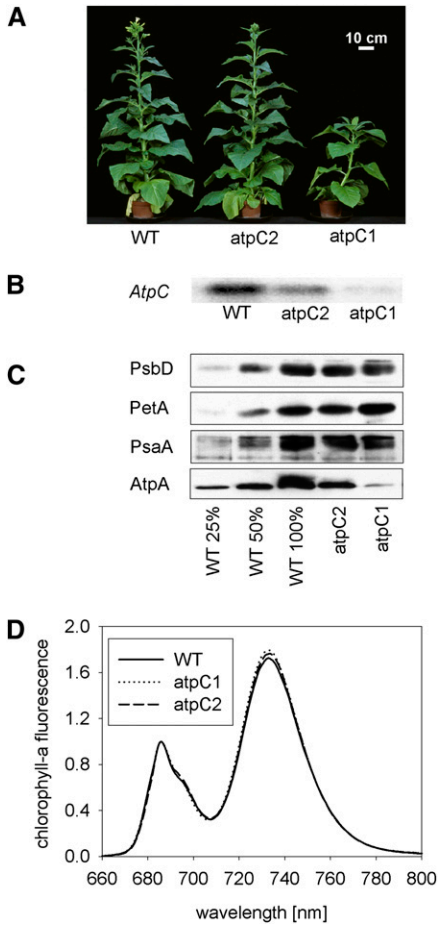

Figure 1. Growth of *AtpC* Antisense Plants Is Retarded Due to a Specific Reduction in ATP Synthase Content.

(A) Growth phenotypes of tobacco wild type (WT) (cultivar SNN) and weak (atpC2) and strong antisense lines (atpC1). Plants were photographed 14 weeks after germination when the wild type started to flower. Bar = 10 cm.

(B) RNA gel blot of *AtpC* mRNA accumulation demonstrating that the strength of the visible phenotype correlates with the degree of *AtpC* mRNA repression.

(C) Protein gel blot analyses of *AtpC* antisense plants. For approximate quantitation, wild-type samples were diluted to 25 and 50%, respectively (lanes 1 and 2), followed by the undiluted wild-type sample and samples from the weak and strong antisense lines. Photosynthetic complex abundance was determined from the contents of essential subunits of PSII (PsbD), cyt-bf (PetA), PSI (PsaA), and the ATP synthase (AtpA).

(D) The 77K chlorophyll-*a* fluorescence emission spectra supporting unaltered antenna distribution between both photosystems in the wild type (filled line), the weak antisense line (long dash), and the strong antisense line (dotted line).

the wild type and the weak atpC2 antisense line, the strong antisense line suffered from a slight reduction in chlorophyll content, which, however, did not significantly alter leaf absorptance. The most pronounced effect in the strong antisense line was a clear reduction in leaf assimilation capacity to ~40% of the levels in the wild type and the atpC2 plants. Respiration was unaltered. The quantum efficiency of CO_2 assimilation, as determined from the linear ranges of light response curves between 0 and 40 μmol photons m^{-2} s^{-1}, was slightly reduced in the strong antisense line.

Interestingly, the chlorophyll *a*/*b* ratio was clearly reduced in the strong atpC1 mutant, suggesting a remodeling of the photosynthetic apparatus. Therefore, photosynthetic complex accumulation was determined spectroscopically. When normalized to chlorophyll content, neither PSII nor cyt-bf contents differ significantly between the wild type and the antisense lines. Also, PSII function does not seem to be impaired in the antisense lines, as indicated by the unaltered F_v/F_m values of dark-adapted leaves (Table 1). Interestingly, PC accumulation was increased to 150% of wild-type levels in the strong antisense line, while its PSI contents were slightly reduced, which concurs with its reduced chlorophyll *a*/*b* ratio (Table 1). These spectroscopic data were independently confirmed by protein gel blots (Figure 1C). No changes in the accumulation of PSII (probed with an antibody directed against the essential reaction center subunit PsbD), cyt-bf (probed with an antibody against the essential PetA subunit), and PSI (probed with an antibody against the essential reaction center subunit PsaA) could be detected. The small decrease of redox-active PSI determined spectroscopically is below the resolution of protein gel blots.

The content of ATP synthase, as determined using an antibody against AtpA, the essential α-subunit of CF1, was clearly diminished in both antisense lines (Figure 1C). While in the weak antisense line atpC2, ATP synthase contents ranging between 100 and ~65% of wild-type levels were observed, the ATP synthase content was much more reduced in the strong antisense line atpC1. In this line, ATP synthase contents ranging between 25 and 10% of the wild-type contents were determined. We only probed a single subunit of the ATP synthase, as loss of all subunits had previously been shown for an *AtpC* knockout line in *Arabidopsis*, indicating that all other subunits are degraded when they cannot assemble together with AtpC into a stable complex (Bosco et al., 2004).

The effects of AtpC suppression on antenna complexes was assessed by 77K chlorophyll-*a* fluorescence emission spectra (Figure 1D), which, in the mutants, do not differ from the wild type, indicating that the strong antisense line can compensate for the small reduction in PSI reaction center contents by an antenna redistribution between both photosystems. In summary, these data suggest that the pronounced growth phenotype of the strong antisense line is specifically attributable to the reduced ATP synthase abundance.

Generation and Molecular Characterization of *atpB* Translation Initiation Mutants

To test an independent set of ATP synthase mutants that do not rely on epigenetic suppression of nuclear gene expression, we also wanted to reduce the expression level of an essential plastid genome-encoded ATP synthase subunit by generating transplastomic tobacco plants. To this end, point mutations were introduced into the AUG translation initiation codon of the *atpB* mRNA. The translation initiation codon is a major determinant of the rate of plastid translation initiation (Sugiura et al., 1998;

Table 1. Photosynthetic Parameters in Wild-Type Tobacco (SNN) and in the *AtpC* Antisense Lines

Parameter	Wild-Type SNN	*atpC1* (Strong Antisense Line)	*atpC2* (Weak Antisense Line)
Chlorophyll *a/b*	4.00 ± 0.19	3.46 ± 0.11	3.92 ± 0.08
Chlorophyll (mg m^{-2})	421.3 ± 82.2	332.0 ± 73.3	460.4 ± 119.6
Leaf absorptance (%)	87.7 ± 2.4	86.4 ± 2.5	88.8 ± 0.9
Assimilation (μmol CO_2 m^{-2} s^{-1})	26.1 ± 3.6	9.9 ± 2.4	24.1 ± 1.7
Respiration (μmol CO_2 m^{-2} s^{-1})	−1.2 ± 0.5	−0.9 ± 0.5	−0.9 ± 0.3
Quanta/CO_2	12.2 ± 2.0	15.3 ± 2.2	13.3 ± 2.3
F_v/F_m	0.83 ± 0.03	0.82 ± 0.02	0.81 ± 0.04
PSII (mmol mol $chlorophyll^{-1}$)	2.67 ± 0.24	2.69 ± 0.16	3.11 ± 0.23
Cyt-bf (mmol mol $chlorophyll^{-1}$)	1.12 ± 0.25	1.15 ± 0.11	1.22 ± 0.19
PC (mmol mol $chlorophyll^{-1}$)	6.91 ± 0.94	9.87 ± 1.27	7.43 ± 0.92
PSI (mmol mol $chlorophyll^{-1}$)	2.38 ± 0.13	1.97 ± 0.12	2.37 ± 0.14
ECS time constant (ms)	23.5 ± 2.8	52.5 ± 17.9	26.6 ± 2.8

All measurements were performed on the youngest fully expanded leaves of plants at the onset of flowering. A minimum of eight plants per line were measured, and the SD is given.

Majeran et al., 2000). In addition to the standard translation initiation codon AUG, two alternative start codons exist in plastids: GUG and UUG. While GUG is used as an initiation codon in both algae and higher plant chloroplasts, UUG has so far been found only in eukaryotic algae (Sugiura et al., 1998; Hirose et al., 1999). In a tobacco in vitro translation system, both alternative start codons can be recognized as translation initiation codons, but their translation initiation efficiency is much lower than that of the standard AUG codon (Hirose et al., 1999; Hirose and Sugiura, 2004). Therefore, transplastomic plants with these point mutations should accumulate reduced amounts of chloroplast ATP synthase.

The TTG and GTG mutations were introduced into a cloned plastid DNA fragment, and a chimeric *aadA* gene was inserted in the intergenic spacer between the *rbcL* gene and *atpB* (Figure 2A). The *aadA* confers resistance to spectinomycin and serves as a selectable marker gene for chloroplast transformation (Svab and Maliga, 1993). The resulting transformation vectors were termed *aadA-atpB* (control construct containing the *aadA* but no mutation in the start codon), TTG-*atpB*, and GTG-*atpB* (Figure 2A). Chloroplast transformation experiments using the biolistic protocol yielded several transplastomic lines, which were purified to homoplasmy by additional selection and regeneration rounds. Two lines per construct were characterized in detail (Figures 2B to 2D). First, homoplasmy of the transformants was confirmed by restriction fragment length polymorphism analysis (Figure 2B). All mutant lines exclusively gave rise to a single hybridization signal of 7.2 kb, strongly suggesting that they were homoplasmic. Subsequently, the homoplasmic presence of the point mutations in the TTG-*atpB* and GTG-*atpB* mutants was confirmed by DNA sequencing. Finally, inheritance tests were performed as the most sensitive approach to distinguish homoplasmy from heteroplasmy (Svab and Maliga, 1993; Bock, 2001). Wild-type seeds germinated on spectinomycin were completely white, while the mutant seedlings were homogeneously green, confirming the homoplasmic state of the transformants.

To characterize *atpB* expression in the transplastomic lines, we first compared transcript accumulation for *atpB*, *rbcL*, *aadA*, and the nuclear-encoded *AtpC* gene by RNA gel blot analysis (Figure 2C). The wild type displayed two similarly abundant bands for the *atpB* transcript, which may be attributable to the presence of multiple promoters upstream of the *atpB* gene (Chen et al., 1990). By contrast, all transformants contained only the shorter *atpB* transcript, which accumulated to similar levels as in the wild type. This indicates that the insertion of the *aadA* selectable marker gene has disrupted one of the *atpB* promoters. Accumulation of the *rbcL* mRNA was unaltered in all transformants, confirming that the insertion of the selectable marker gene between *atpB* and *rbcL* did not interfere with *rbcL* transcript accumulation. As expected, the *aadA* selectable marker gene was strongly expressed in all mutants and not detectable in the wild type. Expression of the nuclear *AtpC* gene was unaltered in all transformants when compared with the wild type.

To assess the effects of the TTG-*atpB* and GTG-*atpB* point mutations on translation, we determined the degree of polysome loading of the *atpB* mRNA as a proxy of translational activity (Barkan, 1998; Figure 2D). Sucrose gradient ultracentrifugation was used to separate mRNAs according to their loading with ribosomes, and six fractions were collected from the gradient after centrifugation. To distinguish between fractions of the sucrose gradient containing free *atpB* mRNA that is not associated with ribosomes and fractions containing the ribosome-associated, actively translated mRNAs, a sample was treated with puromycin, resulting in ribosome dissociation and release of the mRNA. The puromycin control indicates that free mRNAs are strongly enriched in fraction 2 of the sucrose gradient, while almost no signal is obtained for fractions 4 to 6. Therefore, mRNAs found in fractions 4 to 6 are ribosome associated and actively translated.

For the wild type, the strongest mRNA signals were obtained in fractions 4 and 5 (Figure 2D), while considerably weaker signals were detectable in fractions 3 and 6. Both *atpB* transcript species showed the same distribution in the gradient, indicating that their translation efficiency is comparable. The *aadA-atpB* control showed a similar mRNA distribution in the sucrose gradient as the wild type, suggesting that the translation rates are very similar to those in the wild type. The TTG-*atpB* mutation resulted in a clear shift of the polysome profile toward the upper fractions, indicating reduced translational efficiency. However, the strongest signal was still observed in fraction

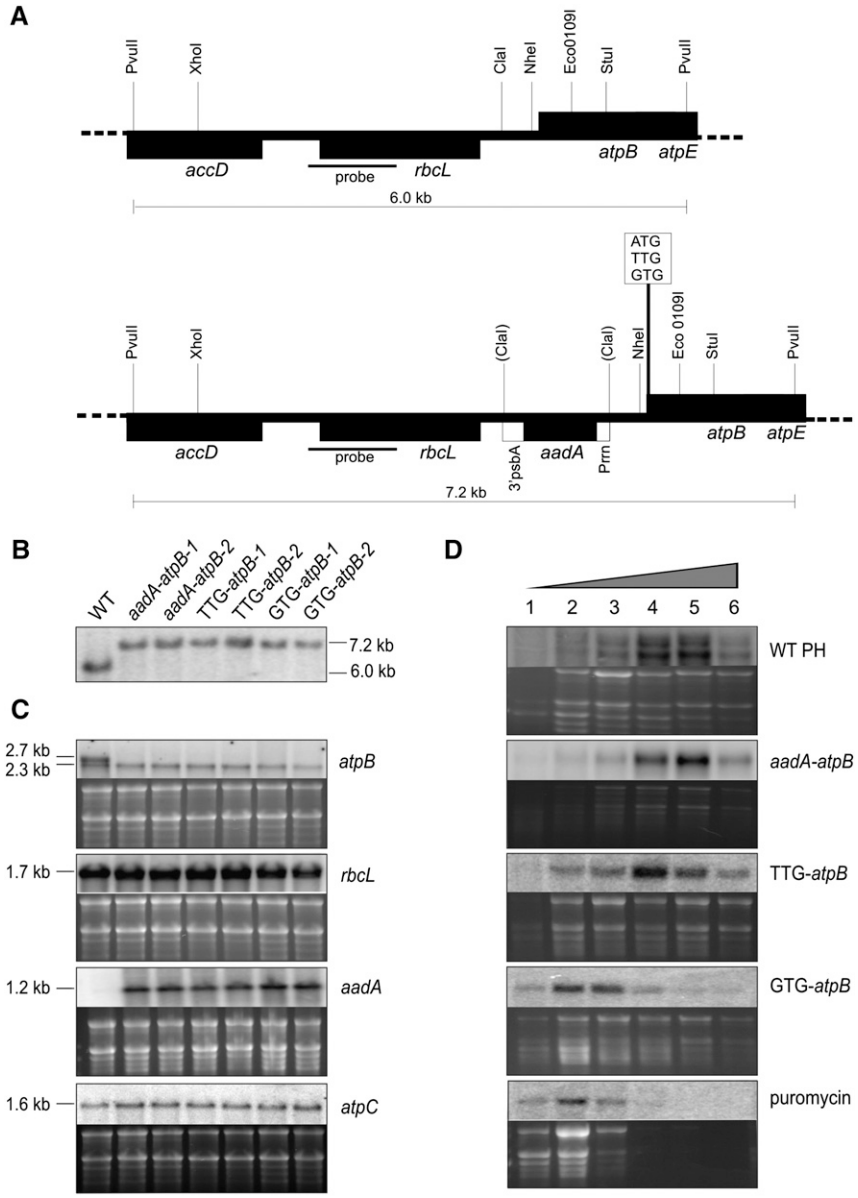

Figure 2. Generation and Molecular Characterization of *atpB* Translation Mutants.

(A) Physical maps of the wild-type plastome region containing *atpB* (top) and the transplastome (bottom). Genes are shown as filled boxes. Genes shown above the line are transcribed from left to right and genes below the line in the opposite direction. Restriction sites used for cloning and restriction fragment length polymorphism analysis are indicated. Sites lost during the cloning process are shown in parentheses.

(B) Restriction fragment length polymorphism analysis of transplastomic plants. DNA was restricted with *Pvu*II. The location of the (*rbcL*-derived) hybridization probe is indicated in **(A)**. The wild type (WT) shows the expected restriction fragment of 6.0 kb, while all transformants show only the transplastomic fragment of 7.2 kb (see **[A]**), confirming their homoplasmic state.

(C) Gene expression analysis in transplastomic plants. Expression of *atpB*, *rbcL* (encoding the large subunit of ribulose-1,5-bisphosphate carboxylase/oxygenase), the selectable marker gene *aadA*, and the nuclear-encoded *AtpC* gene was tested by RNA gel blot analysis.

(D) Polysome loading analysis to determine *atpB* translation rates in the *atpB* start codon mutants. Polysome association of the *atpB* mRNA was determined by fractionation of the sucrose gradient into six fractions. Polysome dissociation induced by puromycin treatment was used to identify fractions containing free mRNAs. These are only found in fractions 1 to 3, indicating that fractions 4 to 6 contain actively translated mRNAs. Fraction numbers are given above (from top to bottom), and the wedge indicates the increasing sucrose concentration in the gradient. The ethidium bromide–stained agarose gel is shown below each blot.

four, suggesting that the majority of the *atpB* mRNA is still translated. By contrast, the GTG-*atpB* mutant showed a severe alteration of the polysome profile. Similar to the puromycin control, signals were only obtained for the upper three fractions (Figure 2D), suggesting that *atpB* translation was largely abolished in this mutant.

In spite of the translational defects in the TTG-*atpB* and especially the GTG-*atpB* mutants, all transformants could grow autotrophically in soil. For Figure 3A, all plants were photographed 12 weeks after germination. While the wild type and the *aadA-atpB* control plants were phenotypically indistinguishable and started to flower, growth of the TTG-*atpB* mutant was clearly retarded. On average, onset of flowering was delayed by 1 week. Growth of the GTG-*atpB* mutant was severely compromised, and the plants flowered only after 6 to 9 months, producing much less flowers and seeds than the wild type and the other mutants. Therefore, the observed growth phenotypes are well in line with the translation rates as estimated from the polysome profiles.

Analysis of the Photosynthetic Apparatus in *atpB* Translation Mutants

To assess the impact of reduced *atpB* translation on the photosynthetic apparatus, the same physiological measurements as described for the *atpC* antisense plants were performed on the youngest fully expanded leaves of plants in the developmental stage shown for the wild type and the *aadA-atpB* control plants in Figure 3A. Interestingly, neither leaf absorptance, chlorophyll content, chlorophyll *a*/*b* ratio, assimilation, respiration, maximum PSII quantum efficiency, nor photosynthetic complex contents showed significant differences between the wild type, the *aadA-atpB* control transformant, and the TTG-*atpB* mutant (Table 2). Only the strongly affected GTG-*atpB* mutant suffered from a >50% reduction of chlorophyll content per leaf area, which also resulted in an ~10% reduction in leaf absorptance (Table 2). Furthermore, its assimilation capacity per leaf area was repressed to 5% of wild-type levels, and respiration was reduced to 40% of wild-type rates. The quantum efficiency of photosynthesis in the GTG-*atpB* mutant was strongly reduced. Assimilation of one CO_2 required 27 quanta, while in the wild type, the *aadA-atpB* control, and the TTG-*atpB* mutant, 11 to 12 quanta per CO_2 were sufficient. Furthermore, the chlorophyll *a*/*b* ratio was strongly reduced in the GTG-*atpB* mutant, which, as in the atpC1 line, is attributable to a diminished accumulation of PSI, while PC contents per chlorophyll were strongly increased (Table 2). Accumulation of cyt-bf and PSII were unaltered. Measurements of the maximum quantum efficiency of PSII indicated that the GTG-*atpB* transformants suffered from mild photoinhibition of PSII.

The spectroscopically determined contents of the photosynthetic complexes were confirmed by protein gel blots (Figure 3B) using the same antibodies as described for the *atpC* antisense plants. In spite of their similar growth phenotype, the *aadA-atpB* control plants showed an ~25% reduction in ATP synthase contents, relative to the wild type. Interestingly, while growth and *atpB* translation rates were clearly reduced in the TTG-*atpB* mutant, ATP synthase levels were indistinguishable from the *aadA-atpB* control (i.e., both had a 25% reduction in ATP synthase contents). ATP synthase accumulation in the strong GTG-*atpB* mutant was repressed to below 10% of wild-type levels, consistent with the strong reduction of both *atpB* translation rates and plant growth.

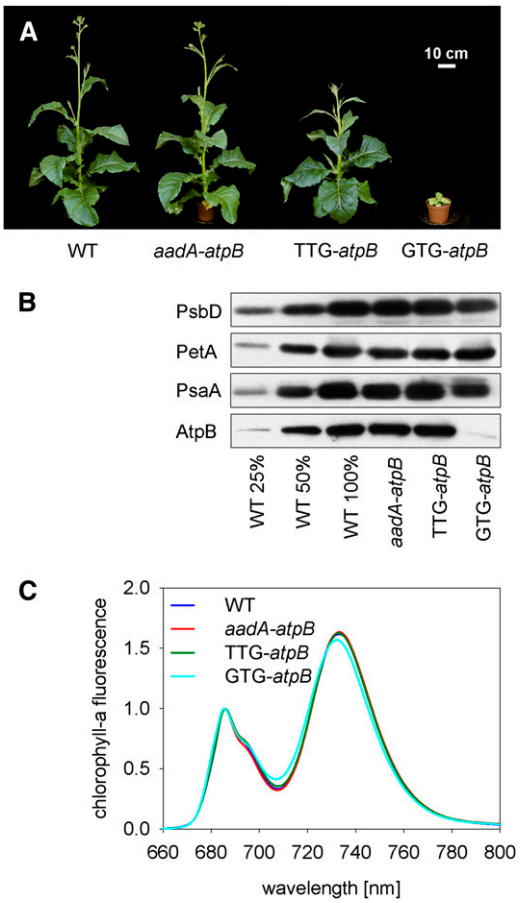

Figure 3. Growth Phenotypes and Composition of the Photosynthetic Apparatus in *atpB* Translation Mutants.

(A) Growth phenotypes of tobacco wild type (WT), *aadA-atpB* control plants, and *atpB* translation mutants. Plants were photographed 12 weeks after germination when the wild type started to flower. Note mild growth reduction and slightly delayed flowering in the TTG-*atpB* mutant but severely retarded growth in the GTG-*atpB* mutant. Bar = 10 cm.

(B) Confirmation of the loss of ATP synthase in the *atpB* translation mutants by protein gel blot analysis. The GTG-*atpB* mutant also shows a small reduction in PSI (PsaA). For approximate quantitation, wild-type samples were diluted to 25 and 50%, respectively (lanes 1 and 2), followed by the undiluted wild-type sample, the *aadA-psaA* control plant, and samples from the TTG-*atpB* and GTG-*atpB* transplastomic lines. Photosynthetic complex abundance was determined from the contents of essential subunits of PSII (PsbD), cyt-bf (PetA), PSI (PsaA), and the ATP synthase (AtpA).

(C) The 77K chlorophyll-*a* fluorescence emission spectra of wild-type tobacco (dark-blue line), the *aadA-atpB* control (red line), the TTG-*atpB* mutant (green line), and the GTG-*atpB* mutant (light-blue line).

Finally, we also recorded the 77K chlorophyll-*a* fluorescence emission spectra (Figure 3C). The fluorescence emission signals of the wild type, *aadA-atpB*, and the TTG-*atpB* mutant were

Table 2. Photosynthetic Parameters in Wild-Type Tobacco (Petit Havana) and in the *atpB* Translation Initiation Mutants

Parameter	Wild-Type PH	*aadA-atpB*	TTG-*atpB*	GTG-*atpB*
Chlorophyll *a/b*	4.02 ± 0.12	3.96 ± 0.09	3.96 ± 0.09	3.17 ± 0.17
Chlorophyll (mg m^{-2})	426.5 ± 30.4	438.5 ± 28.4	457.4 ± 61.7	205.7 ± 57.1
Leaf absorptance (%)	89.4 ± 2.2	87.9 ± 1.8	89.9 ± 1.5	78.1 ± 4.9
Assimilation (μmol CO_2 m^{-2} s^{-1})	30.4 ± 4.1	27.5 ± 2.8	31.1 ± 5.3	1.6 ± 0.6
Respiration (μmol CO_2 m^{-2} s^{-1})	−1.6 ± 0.4	−1.9 ± 0.3	−1.8 ± 0.7	−0.6 ± 0.2
Quanta/CO_2	11.7 ± 1.4	12.3 ± 2.3	11.4 ± 0.9	27.0 ± 5.4
F_v/F_m	0.82 ± 0.02	0.83 ± 0.01	0.84 ± 0.01	0.73 ± 0.04
PSII (mmol mol $chlorophyll^{-1}$)	2.59 ± 0.21	2.57 ± 0.25	2.54 ± 0.24	2.56 ± 0.38
Cyt-bf (mmol mol $chlorophyll^{-1}$)	1.09 ± 0.16	1.01 ± 0.13	1.05 ± 0.17	1.11 ± 0.18
PC (mmol mol $chlorophyll^{-1}$)	4.44 ± 1.42	5.34 ± 1.12	5.16 ± 1.10	9.37 ± 1.28
PSI (mmol mol $chlorophyll^{-1}$)	2.37 ± 0.09	2.39 ± 0.07	2.41 ± 0.07	1.90 ± 0.12
ECS time constant (ms)	22.7 ± 4.1	22.3 ± 2.3	23.6 ± 1.7	90.2 ± 20.8

All measurements were performed on the youngest fully expanded leaves of plants at the onset of flowering. Six wild-type plants and a minimum of four plants per transformant line were measured. As the two independently generated transplastomic lines for each constructs were indistinguishable, average data and the SD from two lines per construct are shown.

indistinguishable, which is consistent with unaltered photosynthetic complex accumulation and chlorophyll *a/b* ratios, suggesting that also their antenna organization is unaltered. By contrast, the strong GTG-*atpB* mutant showed a small shift of the PSI emission maximum from 733- to 731-nm wavelength. This shift is indicative of the presence of light-harvesting complex I proteins uncoupled from PSI, which would be in agreement with the reduced PSI accumulation and the decreased chlorophyll *a/b* ratio (Table 2).

ATP Synthase Activity Strictly Correlates with Linear Electron Flux and Assimilation Capacity but Not with ATP Synthase Contents

To understand the strong effect of ATP synthase repression on growth in both the atpC1 antisense and the GTG-*atpB* translation mutant in more detail, we next determined the ATP synthase activity by means of the fast dark-relaxation kinetics of the maximum electrochromic absorption shift (ECS_T), which represents a measure of the light-induced pmf across the thylakoid membrane (Cruz et al., 2001; Kramer et al., 2003; Takizawa et al., 2007). The relaxation of the pmf upon a light–dark transition is determined mainly by the efflux rate of protons through the ATP synthase and therefore serves as a measure for ATP synthase activity. All measurements were performed under steady state conditions with a fully activated Calvin cycle and in saturating CO_2 to avoid limitation of ATP synthase activity by the metabolic regeneration of ADP and inorganic phosphate.

The average relaxation halftime was 23.5 ms in the wild-type cultivar SNN (Table 1) and nearly unaltered in the weak atpC2 antisense line (26.6 ms), indicating that ATP synthase activity is largely unaffected in fully expanded leaves. In the strong antisense line, the halftime was increased to 53 ms (i.e., ATP synthase activity was reduced to <50% of wild-type levels). Among the *atpB* translation mutants, only the GTG-*atpB* mutant showed a drastic alteration of the pmf relaxation halftime. While the wild type, the *aadA-atpB* control, and the TTG-*atpB* plants all displayed relaxation half-times of 22 to 24 ms, the relaxation halftime was increased to 90 ms in the GTG-*atpB* mutant (Table 2), revealing that thylakoid membrane proton conductivity was reduced to 25% of wild-type values.

To analyze the dependence of ATP synthase activity on ATP synthase content in more detail, we performed quantitative protein gel blots. ATP synthase contents of all samples were normalized relative to the sample with the highest enzyme content. The reciprocal values of the relaxation halftime (e.g., the conductivity of the thylakoid membrane to protons [g_{H^+}], which is proportional to ATP synthase activity) were then plotted as a function of ATP synthase content (Figure 4A). An up to 50% reduction in ATP synthase content does not result in a clear decrease of ATP synthase activity, strongly indicating a complex posttranslational regulation of ATP synthase activity. Only for the atpC1 antisense line and the GTG-*atpB* translation initiation mutant was a clear correlation between content and activity observed.

Next, we analyzed the dependence of assimilation capacities per leaf area (Figure 4B) and linear electron flux (as determined from the quantum yield of PSII after correction for leaf absorptance; Figure 4C) on ATP synthase activity (g_{H^+}). In the GTG-*atpB* mutant and the atpC1 antisense line, a clear correlation between ATP synthase activity, assimilation capacity, and linear electron flux was observed, suggesting that ATP synthase activity is limiting leaf assimilation and controlling electron transport once ATP synthase is strongly repressed.

ATP Synthase Repression Results in Increased Lumen Acidification and Accelerated Induction of Photoprotective Mechanisms

To test if the parallel repression of leaf assimilation and ATP synthase activity is a consequence of a restricted availability of ATP to the Calvin cycle or, alternatively, is due to feedback effects of the reduced thylakoid conductivity on electron transport, we analyzed the responses of linear electron flux and the proton circuit in detail. First, we determined light response curves of the pmf (Figure 5A) and its partitioning into ΔpH and

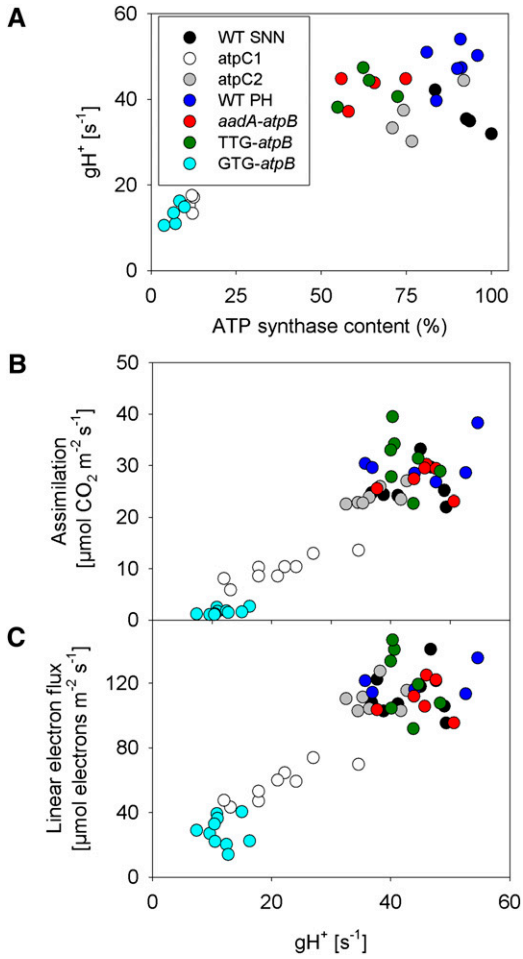

Figure 4. ATP Synthase Activity Limits Assimilation Capacity and Linear Electron Flux.

Each dot in the graphs represents the results for a single plant. Wild-type (WT) SNN plants are shown as black closed circles, the atpC1 plants as black open circles, and the atpC2 plants as gray filled circles. Color usage for the *atpB* translation mutants is as in Figure 3.

(A) ATP synthase activity (g_{H^+}) as a function of ATP synthase content.

(B) Assimilation (expressed on a leaf area basis) as a function of ATP synthase activity (g_{H^+}).

(C) Linear electron flux (on a leaf area basis) as determined from chlorophyll-*a* fluorescence analysis and corrected for leaf absorptance as a function of ATP synthase activity (g_{H^+}).

$\Delta\Psi$ (Figure 5B). The two components of the pmf can be distinguished by measuring the slow phase of ECS relaxation in the range of seconds, which is attributable to slow counter ion movements across the thylakoid membrane and proportional to the ΔpH component (Cruz et al., 2001, Baker et al., 2007). The ECS_T amplitudes clearly show that, as a consequence of the lower thylakoid conductivity in both the strong antisense line and the GTG-*atpB* transformant, the maximum pmf across the thylakoid membrane is strongly increased, and its light response curve is shifted to lower light intensities. In both mutants, pmf was fully light saturated at 500 µmol photons m^{-2} s^{-1}, and already at 200 µmol photons m^{-2} s^{-1} light intensity, >80% of the maximum pmf was established. In the wild-type plants as well as in the *aadA-atpB* control and in the TTG-*atpB* mutant, pmf was only saturated at 2100 µmol photons m^{-2} s^{-1} light intensity. The weak antisense line showed a tendency toward a slightly increased pmf at all light intensities, relative to the wild-type SNN.

While pmf partitioning into ΔpH and $\Delta\Psi$ was not significantly different at saturating light intensities, the pmf partitioning under low light was clearly shifted in favor of the $\Delta\Psi$ component both in the strong antisense lines and the GTG-*atpB* mutant (Figure 5B). However, relative to the wild type, the ΔpH components in the strong antisense line and in the GTG-*atpB* mutant were still 3 and 2 times larger at 200 µmol photons m^{-2} s^{-1}, respectively, resulting in a more acidic thylakoid lumen.

To determine the effects of the increased lumen acidification in atpC1 and GTG-*atpB* mutants on the efficiency of linear electron flux and PSII antenna function, we measured light response curves of linear electron flux and of the chlorophyll-*a* fluorescence parameters qN and qL, which represent measures of the thermal dissipation of excess excitation energy and of the redox state of the PSII acceptor side, respectively (Krause and Weis, 1991; Baker et al., 2007). In agreement with the lower assimilation rates determined by gas exchange measurements (Figure 4, Tables 1 and 2), linear electron transport rates were strongly reduced in the atpC1 antisense line and even more so in the GTG-*atpB* mutant (Figure 6A). The PSII acceptor side was more rapidly reduced already at low light intensities in the atpC1 antisense line and in the GTG-*atpB* mutant, as revealed by their much lower qL values, suggesting an impaired linear electron flux (Figure 6B). Finally, the onset of qN was accelerated in GTG-*atpB* and in both antisense lines, though the effect was much weaker in atpC2 than in atpC1 (Figure 6C). From the more acidic thylakoid lumenal pH in the antisense lines, it was expected that the strong induction of qN in low light is largely attributable to its rapidly reversible qE component (i.e., the thermal dissipation of excitation energy in the PSII antenna by the xanthophyll cycle and the PsbS protein). This was confirmed by analyzing the relaxation of qN during the first 15 min after the end of actinic illumination. In both antisense lines and in the wild type, the vast majority of qN relaxed within 10 min after the end of actinic illumination, confirming that quenching is of the qE type (PSII photoinhibitory quenching, qI, relaxes much more slowly; Krause and Weis, 1991). The same holds true for the *atpB* translation mutants.

The more reduced state of the PSII acceptor side, as deduced from the light response curve of qL (Figure 6B), could either be the consequence of a general reduction of metabolic NADPH consumption due to ATP limitation of the dark metabolism or, alternatively, could be due to impaired linear electron flux from PSII to $NADP^+$ as a result of the more acidic thylakoid lumen. To distinguish between these two possibilities, we next determined the light response behavior of the PSI donor side by quantifying the increase in oxidized inactive PSI with the light intensity (Figure 7A). While the PSII acceptor side and the PQ pool were much more reduced in the strong antisense line and in the GTG-*atpB* mutant than in the respective wild type (Figure 6B), the PSI donor side showed the opposite redox behavior. It was much more oxidized already at low light intensities, indicating a

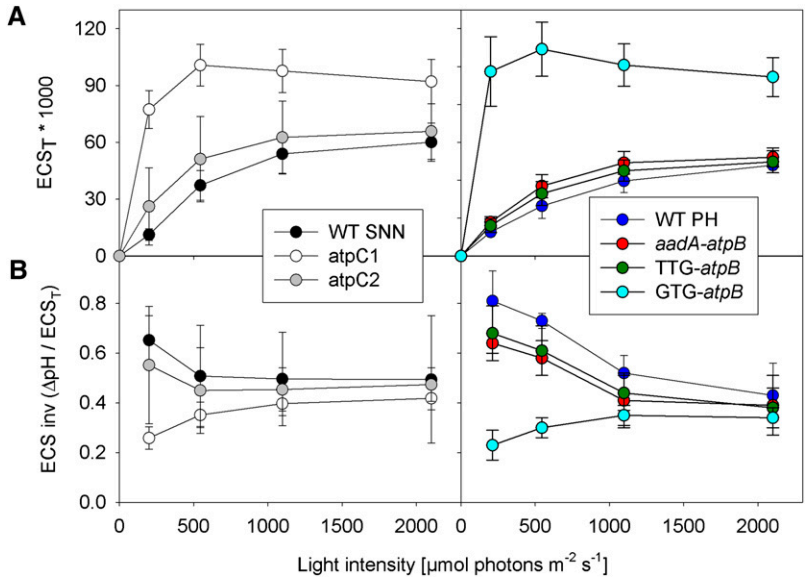

Figure 5. Steady State PMF across the Thylakoid Membrane Is Strongly Increased in the Plants with Diminished ATP Synthase Contents.

Color usage is as in Figures 3 and 4. Data for wild-type (WT) SNN and the antisense lines are shown in the left panel, and data for the wild-type PH and the *atpB* translation mutants are shown in the right panel. A minimum of 10 individual plants was measured per line, and standard deviations are shown as error bars.

(A) Total pmf across the thylakoid membrane as determined from the maximum amplitude of the ECS signal after a light to dark transition (ECS_T) is plotted against the actinic light intensity.

(B) The partitioning of pmf into its ΔpH and $\Delta\Psi$ components is plotted versus the actinic light intensity. Partitioning was determined from the proportion of the slow relaxation kinetics of the ECS attributable to counter ion movements across the thylakoid membrane (ECS_{inv}), relative to ECS_T. While total pmf is strongly increased in the GTG-*atpB* and in the antisense lines, especially at low light intensities, the fraction of pmf stored as ΔpH is slightly reduced.

restricted linear electron flux from PSII toward PSI. No differences between the SNN wild type and the weak antisense line or between the Petit Havana wild type, the *aadA-atpB* control, and the TTG-*atpB* mutant was found (Figure 7A). This strongly suggests that in both the GTG-*atpB* mutant and the strong antisense line, linear electron flux is restricted at the level of cyt-bf or PC.

To determine the exact site of flux limitation, we measured reduction kinetics of cyt-f and P_{700} after the end of a saturating light pulse, when the PSII acceptor side and the PQ pool are completely reduced and the high potential chain comprising cyt-f, PC, and the PSI reaction center chlorophyll-*a* special pair dimer P_{700} is fully oxidized. After the end of the light pulse, electron flux through the cyt-bf toward PSI was determined. For better comparability, the fully oxidized states of cyt-f (Figure 7B) and P_{700} (Figure 7C) were normalized to one, and the completely reduced states were normalized to zero. In agreement with their basically identical light response curves of P_{700} oxidation (Figure 7A), the cyt-f and P_{700} reduction kinetics of the SNN wild type and the weak antisense line were also indistinguishable (with P_{700} reduction half-times being 7 ms). However, the reduction kinetics in the strong antisense line were 2.5-fold slower, with the half-time of P_{700} reduction being increased to 17 ms. This finding is well in line with the observed decrease of leaf assimilation and linear electron flux rates (Figures 4A and 4B) and the altered redox poise of the electron transport chain (Figures 6B and 7A). The same is true for the GTG-*atpB* mutant, whose P_{700} reduction half-time was increased to 22 ms compared with 6 ms in the PH wild type, the *aadA-atpB* control, and the TTG-*atpB* mutant. This is again in good agreement with the strong repression of linear electron flux and assimilation.

DISCUSSION

Modification of Chloroplast ATP Synthase Accumulation by *AtpC* Antisense Repression and Manipulation of *atpB* Translation

In the unicellular green alga *C. reinhardtii*, the accumulation of the chloroplast ATP synthase is controlled in part by the synthesis of the nuclear-encoded γ-subunit. In its absence, translation of the plastid-encoded β-subunit (*atpB*) is repressed (Drapier et al., 2007). As accumulation of the β-subunit is required to activate translation of the α-subunit of the ATP synthase, *atpC* and *atpB* function as dominant subunits in a network of translational autoregulation of ATP synthase biogenesis in *C. reinhardtii*. It is currently unknown if the same mechanisms control ATP synthase biogenesis in higher plants. In this work, we targeted both *atpC* (by a nuclear antisense approach) and *atpB* (by reducing its translation initiation in the chloroplast) to repress ATP synthase accumulation in tobacco and study the impact on photosynthesis, assimilation, and plant growth.

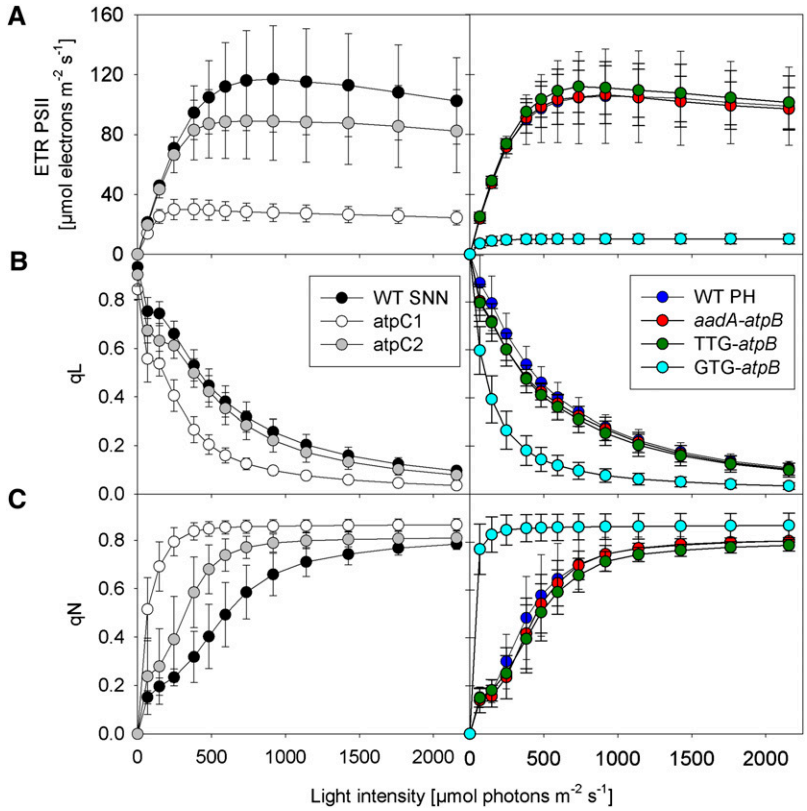

Figure 6. Restricted Linear Electron Transport, Overreduction of the PSII Acceptor Side, and Accelerated Induction of qN upon ATP Synthase Repression.

Symbols are used as in Figure 4. Data for the SNN wild type (WT) and the antisense plants are shown in the left panel, and data for the PH wild type and the *atpB* translation mutants are shown in the right panel. A minimum of 10 individual plants were measured per line, and standard deviations are shown as error bars.

(A) Light saturation curve of linear electron flux as calculated from PSII yield measurements and corrected for leaf absorptance. Linear electron flux is strongly repressed in response to reduced ATP synthase contents.

(B) Redox state of the PSII acceptor side, determined as qL. With increasing light intensity, the PSII acceptor side becomes progressively reduced. Note that this effect is shifted to lower light intensities in the strong antisense line and in GTG-*atpB*.

(C) Measurement of nonphotochemical quenching (qN). The onset of qN is shifted toward lower light intensities in both antisense lines and in the GTG-*atpB* mutant, resulting in increased thermal dissipation of excitation energy, reduced quantum efficiency of photosynthesis, and, thus, lower light use efficiency.

Our data show that both *AtpC* antisense repression and manipulation of *atpB* translation initiation are feasible strategies to modify chloroplast ATP synthase accumulation. The successful repression of ATP synthase accumulation in our transplastomic approach demonstrates that photosynthetic complex contents in higher plants can be altered by reducing translation of an essential subunit.

In vitro translation assays suggested that both UUG and GUG can serve as alternative start codons in chloroplast translation initiation but are recognized with much lower efficiency than the standard AUG initiator codon (Hirose et al., 1999; Hirose and Sugiura, 2004). However, an exact prediction of in vivo translation initiation rates for these alternative start codons is not possible because their efficiency depends strongly on the sequence context around the initiation codon (Boeck and Kolakofsky, 1994). In our experiments, only the GTG-*atpB* transplastomic lines suffered from a strong repression of ATP synthase accumulation, assimilation, and linear electron flux (Figure 4) and displayed strongly retarded growth (Figure 3A). Mature leaves of both the TTG-*atpB* mutant and the *aadA-atpB* control showed on average a 25% reduction of ATP synthase contents, relative to the wild type (Figure 4A). However, this did not result in a significantly reduced ATP synthase activity. Also, no alterations in electron transport and assimilation capacities were observed (Figures 4B and 4C), and all other photosynthetic parameters were indistinguishable from the control plants (Table 2).

The reduced ATP synthase accumulation in both the *aadA-atpB* control and the TTG-*atpB* mutant is most likely attributable to the 50% reduction in *atpB* mRNA accumulation observed in all *atpB* translation initiation mutants. The reduced mRNA accumulation is due to the disruption of a second, so far unknown *atpB* promoter in the tobacco plastome by the insertion of the *aadA*

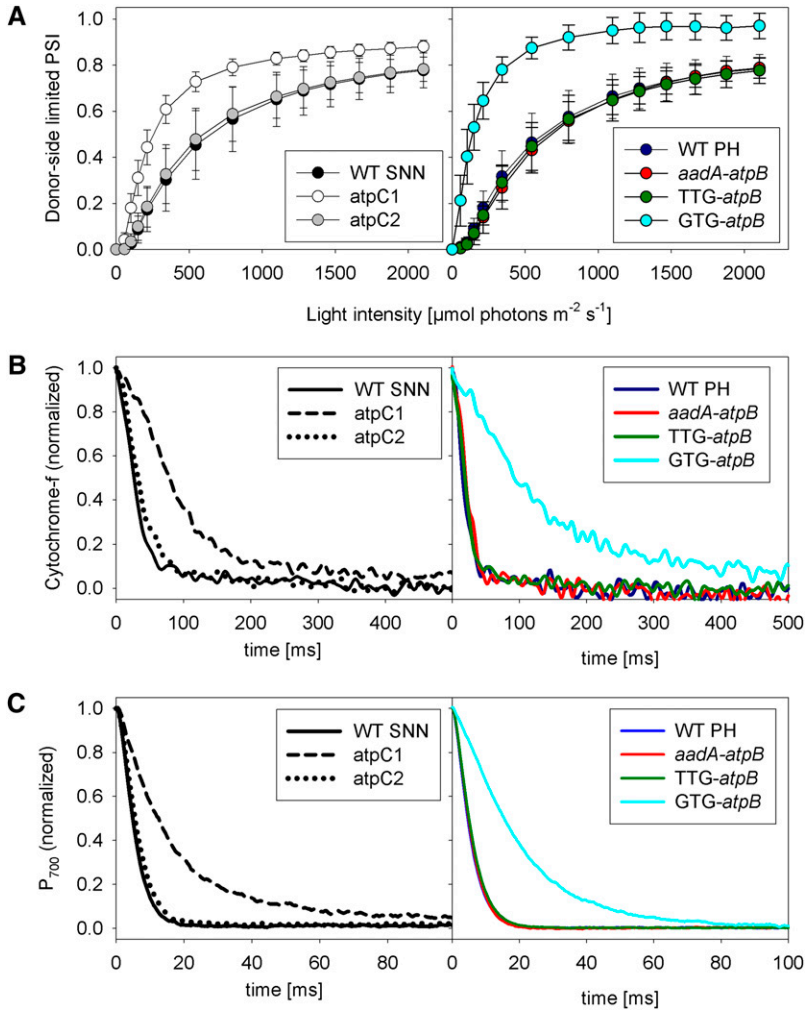

Figure 7. Limited Linear Electron Flux through cyt-bf in ATP Synthase Mutants.

The symbols are used as in Figure 4. Data for the SNN wild type (WT) and the antisense plants are shown in the left panel, and data for the PH wild type and the *atpB* translation mutants are shown in the right panel. A minimum of 10 individual plants were measured for all lines, and standard deviations are shown as error bars in **(A)**.

(A) Light intensity–dependent oxidation of the donor side of PSI and the high potential chain.

(B) and **(C)** Restricted linear electron flux due to photosynthetic control, as evidenced by retarded reduction kinetics of cyt-f **(B)** and P_{700} **(C)**.

selectable marker gene (Figure 2C). It is not surprising that the actual ATP synthase accumulation in the *aadA-atpB* control and the TTG-*atpB* mutant is much less affected than *atpB* mRNA levels, as it is well established that translation initiation rather than transcription is limiting photosynthetic complex accumulation in photosynthetic eukaryotes (Eberhard et al., 2002; Drapier et al., 2007).

Interestingly, polysome analyses revealed that also in the TTG-*atpB* mutant, *atpB* translation was somewhat reduced, relative to the wild type and the *aadA-atpB* control, even though the effects were much less severe than those in the GTG-*atpB* mutant, in which *atpB* translation was almost completely abolished. This slight reduction of *atpB* translation in the TTG-*atpB* mutant might explain the weak growth retardation relative to the *aadA-atpB* control, which displayed a similar (~25%) reduction in ATP synthase contents in mature leaves as the TTG-*atpB* mutant. The reduced *atpB* translation could slightly delay ATP synthase biogenesis during the early stages of leaf development, when translation rates are highest. This would limit photosynthesis during early phases of plant development, when growth is most sensitive to delayed establishment of a fully functional photosynthetic apparatus and reduced photoassimilate availability. In mature leaves, when the photosynthetic apparatus is fully established and low translation rates are sufficient for its maintenance, ATP synthase contents then reach wild-type levels. Due to the limited availability of young, strongly expanding leaf material, we have not yet been able to test this hypothesis.

As a second independent approach and to obtain mutants covering a wider range of ATP synthase contents, we also used antisense RNA directed against the nuclear-encoded essential

AtpC subunit. We analyzed two lines suffering from different degrees of ATP synthase repression in detail. One of the lines (atpC1) showed a strong growth phenotype and a clear reduction in ATP synthase accumulation, providing ATP synthase activities between those of the GTG-*atpB* translation mutant and the wild type. The other line (atpC2) showed only a mild reduction in ATP synthase accumulation, and linear electron flux and assimilation were largely unaltered relative to the wild type. Taking the translation initiation mutants and the antisense plants together, a wide range of ATP synthase contents and activities is covered.

One concern arising from employing an antisense strategy is the possibility that the observed phenotypes are not exclusively related to the repression of the target gene. In theory, other genes could be affected by so-called off-target effects. These could be brought about by posttranscriptional silencing of genes sharing short identical sequence stretches with the gene of interest. As the tobacco genome is not fully sequenced, it is not possible to fully exclude such off-target effects. However, two lines of evidence argue against the presence of off-target effects in our nuclear-transgenic antisense plants. First, no EST from tobacco or any other Solanaceous species was found that would share homologous sequences of >18 bp length with *AtpC*. More importantly, comparison of phenotypes and photosynthetic parameters in nuclear antisense and the plastid translation mutants provides strong evidence against off-target effects. The GTG-*atpB* and atpC1 mutants behave in a very similar manner, as far as the effects of reduced ATP synthase activity on linear electron transport and leaf assimilation capacity are concerned (Figures 4B and 4C), with all parameters being slightly more affected in the GTG-*atpB* mutant due to its more severe ATP synthase repression. Both mutants also suffer from an accelerated induction of qN already at low light intensities (Figure 6C) due to increased lumen acidification (Figures 5A and 5B), resulting in a decreased quantum efficiency of CO_2 fixation (Tables 1 and 2). They also suffer from a chronic overreduction of the PSII acceptor side (Figure 6B) and an accelerated oxidation of the PSI donor side (Figure 7A) due to decreased rates of PQ reoxidation at the cyt-bf (Figures 7B and 7C). Finally, both mutants also show a reduced PSI accumulation and an upregulation of PC (see below). Therefore, the observed effects are independent of the chosen strategy for ATP synthase repression.

Decreasing ATP Synthase Contents Reduces CO_2 Assimilation, Electron Transfer, and Plant Growth

ATP synthase repression to <50% of wild-type levels resulted in a marked reduction of ATP synthase activity. Strikingly, we observed a strict correlation between the activity of the ATP synthase, measured by the decay of the ECS signal, and assimilation capacity (Figure 4B) as well as linear electron flow (Figure 4C), establishing ATP synthase activity as a potentially limiting or governing factor of photosynthesis. This observation is in agreement with the growth phenotypes reported by Price et al. (1995) for δ-subunit antisense lines, although at that time, no analysis of the molecular mechanisms underlying the growth retardation was undertaken. It has also been observed that mutations affected in the reductive activation of the ATP synthase by thioredoxin (due to amino acid substitutions in the γ-subunit) have an adverse effect on photosynthesis and plant growth in low light (Wu et al., 2007), although also in this case, the mechanistic basis has not been explored.

Steady State pmf Is Increased in ATP Synthase Mutants

In vivo probing of both electron and proton transfer allowed us to follow the effects of reduced ATP synthase expression on the photosynthetic energy budget. We found that reduced ATP synthase activity leads to an increased steady state pmf (Figure 5A). Even though the partitioning of pmf into $\Delta\psi$ and ΔpH components was shifted in favor of $\Delta\Psi$ in both atpC1 and GTG-*atpB*, especially at low light intensities (Figure 5B), the strongly increased pmf led to a higher ΔpH and thus a more acidic lumenal pH.

Thus, it appears likely that the growth phenotype of the strong antisense plant represents an indirect inhibition of linear electron flux by the increased acidification of the lumen due to restricted PQ reoxidation, a phenomenon referred to as photosynthetic control (Figures 7B and 7C). PQ oxidation represents a rate-limiting step in linear electron flux, even in wild-type plants under nonstressed conditions (Anderson, 1992; Price et al., 1998), but it is further slowed down when the pH value in the thylakoid lumen drops below 6.5. This is because PQ oxidation now works against a much higher preestablished pmf (Kramer et al., 1999; Hope, 2000). Supporting this view, ATP synthase repression led to a more reduced PQ pool (Figure 6B) and a more oxidized high potential chain (Figure 7A), clearly indicating a restriction in electron flow at the level of cyt-bf. The colimitation (or coregulation) of proton flow through the ATP synthase and electron flow through the photosynthetic chain should result in restrictions in both ATP and NADPH synthesis, which in turn result in downregulation of the Calvin cycle.

Excess ATP Synthase Capacity in Wild-Type Plants

Interestingly, neither antisense line atpC2 nor the *aadA-atpB* control or the TTG-*atpB* mutant, which suffer from an up to 40% reduction in ATP synthase contents, displayed a significant decrease in ATP synthase activity (Figure 4A) and assimilation capacity (Figure 4B). Only in the GTG-*atpB* mutant and the strong antisense line atpC1, which contain ATP synthase contents between 20 and <5% of wild-type levels, were clear correlations between ATP synthase content and activity observed. We conclude that ATP synthase activity is not exclusively controlled by absolute enzyme contents but instead is highly regulated at the level of enzyme activity. This was previously demonstrated by Kanazawa and Kramer (2002), showing strong effects of CO_2 levels on ATP synthase activity. When CO_2 was increased from 0 to 2000 ppm, ATP synthase activity increased by approximately sixfold, leading to large changes in the regulation of photosynthesis. It is noteworthy that the maximum ATP synthase activity was not yet reached at 350 ppm CO_2, implying that ATP synthase is partly downregulated at ambient CO_2. Maximum ATP synthase activity was established at 500 ppm CO_2, followed by a minor decrease when CO_2 contents were further increased up to 2000 ppm (Kiirats et al., 2009). All these data suggest that the ATP

synthase is dynamically regulated, and significant reductions in complex content can be compensated by upregulating the enzymatic activity.

The mechanism underlying this dynamic regulation of ATP synthase activity is still not fully understood. One well-established level of ATP synthase regulation is its reductive activation via the thioredoxin system, which has strong effects on enzyme activity. The oxidized enzyme operates at <20% of the rate of the fully activated, reduced form (Wu and Ort, 2008). However, as quantitative reduction of the γ-subunit occurs already after short illumination at low light intensities (Wu and Ort, 2008), this reductive activation is unlikely to account for the discrepancy between ATP synthase content and activity under the light-saturated conditions measured here.

It has been suggested that stromal inorganic phosphate levels, modulated by metabolic processes, may regulate ATP synthase activity (Sharkey and Vanderveer, 1989; Takizawa et al., 2008). However, our measurements were performed in saturating CO_2 and after full activation of the Calvin cycle to ensure rapid metabolic consumption of ATP and NADPH. Therefore, a phosphate limitation is unlikely to significantly contribute to the downregulation of ATP synthase activity in our experiments. The catalytic β-subunit of the ATP synthase is known to contain several phosphorylation sites (del Riego et al., 2006; Reiland et al., 2009). While two of the sites show strong changes in phosphorylation between day and night and thus could be involved in the nocturnal inactivation of ATP synthase, a third phosphorylation site may be involved in binding of 14-3-3 proteins, which can drastically reduce ATP synthase activity in vitro (Bunney et al., 2001). Therefore, this site seems to be the strongest candidate for regulating ATP synthase activity in the light. However, so far, no direct effect of phosphorylation on ATP synthase activity has been demonstrated in vivo. Furthermore, a metabolically controlled dimerization of the *C. reinhardtii* plastid ATP synthase has been shown (Schwassmann et al., 2007), but an effect on enzyme activity has not been demonstrated yet. Therefore, the reason for the discrepancy between the downregulation of the ATP synthase contents and the less pronounced reduction in activity currently cannot be fully resolved. In this context, it would be interesting to investigate if phosphorylation and/or oligomerization of the ATP synthase differ between the wild type and our transformants with decreased ATP synthase accumulation.

Sensitivity of the Photosynthetic Apparatus to Increased Lumenal Acidification

Under the conditions tested here, we observed no strong increase in photosensitivity in our ATP synthase mutants. The maximum variable PSII fluorescence (F_v/F_m) in the strong antisense line atpC1 was indistinguishable from that in the wild type (Table 1). Also, the GTG-*atpB* mutant suffering from the most pronounced reduction in ATP synthase content and linear electron flux displayed only a mild reduction of F_v/F_m. These results imply that neither the increase in Q_A reduction (Figure 6B) nor the increased lumenal acidification (Figure 5) result in photodamage that would exceed the repair capacity of the chloroplast (Aro et al., 2005).

Lumenal pH values below 5.5 have been observed to dramatically accelerate photodamage in vitro, particularly at the donor side of PSII (Krieger and Weis, 1993; Kramer et al., 1999). Also, PC is highly sensitive to pH values below 5.5 (Gross et al., 1994; Kramer et al., 1999). However, in both the strong antisense line and the GTG-*atpB* mutant, the content of redox-active PC actually increased (Tables 1 and 2). The fact that we observed neither increased PSII photodamage nor inactivation of PC suggests that the lumenal pH did not decrease below this threshold value. Alternatively, the tobacco photosynthetic apparatus might be unusually acid resistant. At present, we favor the former scenario, noting that the pH sensitivity of cyt-bf should act as a feedback regulator preventing overacidification by slowing down electron transfer as pH decreases. Likewise, increased lumenal acidification also activates photoprotective qE quenching (Figure 6C), thereby at least partly ameliorating the photoinhibitory effects of a more reduced PQ pool (Figure 6B). Therefore, the lack of pronounced photodamage in the strong ATP synthase mutants is broadly in line with the proposed role of the ATP synthase in coregulating the light reactions by decreasing electron transfer and triggering antenna downregulation (Takizawa et al., 2007).

The increase in redox-active PC can most likely be attributed to the strongly repressed assimilation capacity of the mutants. PC expression is known to be repressed via sugar sensing when high amounts of photoassimilate accumulate in source leaves (Oswald et al., 2001; Schöttler et al., 2004). Thus, the strongly restricted assimilation in both mutants could result in a derepression of PC. Interestingly, while PC accumulation was increased and neither accumulation nor functional integrity of PSII was strongly affected, both the atpC1 and the GTG-*atpB* mutants suffered from a 20% reduction of redox-active PSI per chlorophyll (Tables 1 and 2). This could indicate that PSI represents the component of the photosynthetic apparatus that is most sensitive to lumenal acidification.

Alternatively, the observed PSI repression could be due to retrograde signals elicited by the repression of ATP synthase. However, the observed repression of PSI cannot be reconciled with any of the known retrograde signals, which should rather result in an upregulation of PSI in the mutants because their PQ pool is chronically overreduced. This should increase PSI contents and repress PSII accumulation because a reduced PQ pool stimulates transcription of the genes for the PSI reaction center subunits *psaA* and *psaB* and represses the expression of PSII reaction center subunits to counteract the redox imbalance (Pfannschmidt et al., 1999, 2009). Likewise, redox signals originating from the more oxidized stroma or from the altered metabolic state should rather activate than repress PSI biogenesis (Pogson et al., 2008; Pfannschmidt et al., 2009). An attractive alternative possibility would be direct signaling from the pmf or the acidified thylakoid lumen. However, no clear evidence for such a signaling mechanism has been obtained to date, and at least expression of the nuclear *AtpC* gene (Figure 2C) would not be a major target of such a pathway because it was unaltered in the *atpB* translation mutants. Future investigations should reveal if the reduced PSI accumulation is attributable to direct damage by increased lumenal acidification or rather to altered photosynthetic gene expression.

The ATP Synthase as a Potent Control Point for Photosynthesis

Our data establish the ATP synthase as an additional control point of the photosynthetic light reactions, as previously suggested by Kramer et al. (2003), in addition to cyt-bf (Anderson, 1992; Price et al., 1995; Kirchhoff et al., 2000) and potentially PC (Schöttler et al., 2004). However, while already very small changes in cyt-bf content and activity linearly affect linear electron flux and assimilation (Price et al., 1998; Kirchhoff et al., 2000), an up to 50% decrease in ATP synthase content can be compensated on a posttranslational level. The relevance of ATP synthase adjustment is obvious from the fact that an up to fivefold downregulation of ATP synthase contents occur during leaf ageing (Schöttler et al., 2007a) and in response to drought stress (Tezara et al., 1999; Kohzuma et al., 2009). Flux control by such strong changes could be even more efficient than by downregulation of cyt-bf. While cyt-bf and PC repression would reduce linear flux directly, ATP synthase regulation would reduce it indirectly due to increased pmf across the thylakoid membrane and photosynthetic control.

However, upon ATP synthase repression, the onset of photoprotective mechanisms is shifted to lower light intensities because lower proton influx rates can sufficiently acidify the lumen to trigger qN. This results in a decrease of the photosynthetic quantum efficiency and thus reduces plant growth. By contrast, selective suppression of cyt-bf without a parallel downregulation of the ATP synthase should have a lower impact on quantum efficiency because it reduces only the capacity for proton influx into the lumen, whereas proton efflux through the ATP synthase would remain high. This should result in a lower steady state pmf and, consequently, in a less efficient induction of the photoprotective mechanisms. Evidence for this scenario comes from our characterization of a Δ*petL* mutant suffering from accelerated leaf age-dependent loss of cyt-bf and reduced electron flux capacity due to absence of a small subunit of the cyt-bf. As the ATP synthase is not degraded in parallel with cyt-bf, but instead maintained at wild-type levels, nonphotochemical quenching in these mutants is compromised (Schöttler et al., 2007b).

By a strict coregulation of ATP synthase and cyt-bf contents during leaf ageing in tobacco (Schöttler et al., 2007a), plants can balance the rates of proton influx via electron transport and proton efflux through the ATP synthase in a way that under nonstressed conditions lumen acidification is kept close to but above the threshold value for triggering photoprotective mechanisms, such as qN and photosynthetic control. In this way, optimum photosynthesis with a high quantum efficiency is ensured. However, when ATP and NADPH consumption by the Calvin cycle decreases, the reduced proton efflux through the ATP synthase results in an immediate decrease of the lumenal pH below the threshold value for activation of the photoprotective mechanisms, thus enabling a rapid response of the plant to this disturbance. Therefore, we postulate ATP synthase as a major control point in the long-term adjustment of the photosynthetic light reactions to changing metabolic demands. Furthermore, we suggest that coregulation of linear electron flux (via cyt-bf and PC contents) with the proton circuit (via ATP synthase accumulation) is required to maintain an optimum steady state lumenal pH value under unstressed conditions. This mechanism allows the plant to tightly control the induction of photoprotective mechanisms, thus optimizing photosynthetic quantum efficiency.

METHODS

Plant Material and Growth Conditions

Tobacco (*Nicotiana tabacum*) *AtpC* antisense lines were raised from seeds germinated on Petri dishes containing Murashige and Skoog medium supplemented with 2% (w/v) sucrose and 300 μg mL^{-1} kanamycin. Wild-type seedlings were grown on the medium without kanamycin. Fourteen days after germination, the seedlings were transferred to a soil-vermiculite mixture (2:1; Floragard Vertriebs) and grown in a controlled-environment chamber. Transplastomic plants were grown on soil. All plants were fertilized with Hakaphos Special (Compo Expert) to keep the soil moist. All measurements were performed on the youngest fully expanded leaves at the onset of flowering. The actinic light intensity was 300 μmol photons m^{-2} s^{-1} at the level of these leaves. The plants were illuminated for 16 h at 22°C. The growth temperature was reduced to 18°C during the night. Relative humidity was set to 75%.

Generation of Antisense Constructs and Nuclear Transformation

The antisense construct was expressed under the control of the cauliflower mosaic virus 35S promoter and assembled in a plasmid vector described previously (Lein et al., 2008). Correct insertion of the cassette was verified by PCR with genomic DNA as template and primers 35S (5′-GTGGATTGATGTGATATCTCC-3′) and octopine synthase (5′-GTAAGGATCTGAGCTACACAT-3′) followed by direct sequencing of the PCR products (Lein et al., 2008). Tobacco plants (cv Samsun NN) were transformed with the antisense construct by *Agrobacterium tumefaciens*–mediated gene transfer using *A. tumefaciens* strain C58C1:pGV2260 (Rosahl et al., 1987).

Vector Construction for Plastid Transformation and Generation of Transplastomic Plants

The region of the tobacco plastid genome containing part of the *accD* gene, the large subunit of ribulose-1,5-bisphosphate carboxylase/oxygenase (*rbcL*), and the 5′ portion of the *atpB* gene was isolated as a 5132-bp *Xho*I/*Stu*I restriction fragment corresponding to plastome positions 55360 to 60492 (Figure 2A). The fragment was cloned into a pBS SK vector (Stratagene) cut with *Xho*I and *Ecl*136II. To remove the *Eco*0109I site from the remaining multiple cloning site, the resulting plasmid was linearized with *Eco*0109I, and the recessed ends were filled in using the Klenow enzyme followed by religation. A chimeric *aadA* gene fused to chloroplast-specific expression signals and conferring resistance to the aminoglycoside antibiotics spectinomycin and streptomycin (Svab and Maliga, 1993) was cloned into a unique *Cla*I site (position 57175) to enable selection of transplastomic lines. Constructs containing the *aadA* selectable marker gene in the same orientation as the *rbcL* gene were chosen for all further cloning steps. This construct was called *aadA-atpB*, as it contained the selectable marker gene and the *atpB* gene without any point mutations in its translation initiation codon.

The *aadA-atpB* construct was then used to produce the translation initiation codon mutations by PCR. The region surrounding the ATG start codon was excised by digestion with *Nhe*I and *Eco*0109I (restriction sites correspond to nucleotide positions 56844 and 56410, respectively) and replaced by PCR products carrying the point mutations. The mutations were introduced with the primer sequences (see below), yielding the final transformation vectors TTG-*atpB* and GTG-*atpB*. Primer oMR1_pMR111_fw

was used to generate the ATG-to-TTG mutation (5′-GTGCTAGCGGACATTTATTTTGAATTCGATAATTTTTGCAAAAACATTTCGACATATTTATTTATTTTATTATT**TTG**AG-3′), primer oMR2_pMR112_fw was used for the ATG-to-GTG mutation (5′-GTGCTAGCGGAATTTATTTTGAATTCGATAATTTTTGCAAAAACATTTCGACATATTTATTTATTTTATTATT**GTG**AG-3′), and primer oMR8_pMR110_bw was used as the reverse primer for both PCR amplifications (5′-GCGCAGATCTATGAATAGGA-3′).

Young sterile leaves of tobacco cultivar PH were bombarded with the respective transformation vectors bound to gold particles (0.6-μm diameter) using a helium-driven biolistic gun (PDS-1000 He; Bio-Rad). Primary transformants were selected from 5 × 5-mm leaf pieces on plant regeneration medium containing 500 mg/L spectinomycin. Several independent transplastomic lines were then subjected to a maximum of three additional rounds of regeneration on spectinomycin-containing medium to enrich for the transplastome and select against residual copies of the wild-type plastome. Spontaneous spectinomycin-resistant lines were eliminated via double selection on media containing both spectinomycin and streptomycin in a concentration of 500 mg/L each (Svab and Maliga, 1993; Bock 2001). Homoplasmic transplastomic lines were transferred to the greenhouse for seed production. The presence of the point mutations in the TTG-*atpB* and GTG-*atpB* mutants was confirmed by DNA sequencing.

DNA Gel Blot and RNA Gel Blot Analyses

Total plant DNA was isolated by a rapid cetyltrimethylammoniumbromide-based miniprep procedure (Doyle and Doyle, 1990). DNA samples digested with restriction enzymes were separated in 0.8 to 1.0% agarose gels and blotted onto Hybond-XL nylon membranes (GE Healthcare) according to the manufacturer's instructions. RNA was extracted from leaves using the peqGold Trifast reagent (Peqlab). Samples equivalent to 2.5 μg RNA were separated in 1% formaldehyde-containing agarose gels and blotted onto Hybond-XL nylon membranes. For hybridization, α[^{32}P] dCTP-labeled probes were generated by random priming (Multiprime DNA labeling kit; GE Healthcare). Hybridizations were performed at 65°C in rapid hybridization buffer (GE Healthcare) following the manufacturer's protocol. An *AtpC*-specific probe was generated by PCR amplification from genomic DNA with the primers OMR14 (5′-GAGGCTATGAAGCTTGTTGC-3′) and OMR15 (5′-GGAAGCAGGGTGTGAATCAC-3′). Hybridizations were performed at 65°C in Rapid-Hyb buffer (Amersham Biosciences) following the protocol of the manufacturer. Hybridization signals were quantified using a Typhoon Trio+ variable mode imager (Amersham Biosciences) and Image Quant 5.2 software.

Polysome Analysis

Polysome-associated mRNAs were isolated from leaves and separated in sucrose gradients as described previously (Rogalski et al., 2008). The sucrose gradients were fractionated, and the RNA precipitated from each fraction and dissolved in 30 μL of water. Eight-microliter aliquots were denaturated for 5 min at 95°C and loaded onto formaldehyde-containing denaturing agarose gels. After electrophoretic separation, RNAs were transferred to membranes as described above.

Gas Exchange Measurements

Leaf assimilation and linear electron flux were measured using the GFS-3000FL gas exchange system equipped with the standard measuring head 3010-S (8-cm^2 leaf area) and the LED-Array/PAM fluorometer module 3055-FL for actinic illumination and chlorophyll-*a* fluorescence determination on intact tobacco plants (Heinz Walz). Light response curves of CO_2 fixation were measured at 20°C cuvette temperature and 17,500 ppm humidity in 2000 ppm CO_2. The light intensity was stepwise increased from 0 to 2000 μmol photons m^{-2} s^{-1}, and at each light intensity, gas exchange was recorded until a steady state of transpiration and stomatal responses was achieved (i.e., for between 30 and 45 min). The quantum efficiency of CO_2 fixation was determined in the linear light response range between 0 and 60 μmol photons m^{-2} s^{-1} (wild type and weak mutants) or between 0 and 40 μmol photons m^{-2} s^{-1} (strong mutants). After the end of the gas exchange measurements, leaf absorptance was determined using an integrating sphere (ISV-469; Jasco) attached to the V550 spectrophotometer (Jasco). The spectral bandwidth was set to 1 nm, and the scanning speed was 200 nm min^{-1}. The transmission and reflectance spectra were measured between 700- and 400-nm wavelength, and leaf absorptance was calculated as 100% – transmittance (%) – reflectance (%). Finally, the chlorophyll content of the measured leaf discs was determined according to Porra et al. (1989). Assimilation rates were corrected for the dark respiration, assuming comparable respiratory activities in the light and in darkness (Fernie et al., 2004).

pmf Measurements and ATP Synthase Activity

The electrochromic absorption shift (ECS) was used as an in vivo probe of the pmf across the thylakoid membrane (Kramer et al., 2003; Takizawa et al., 2007). The difference transmission signal was measured using a KLAS-100 LED-array spectrophotometer (Heinz Walz), allowing the simultaneous measurement of light-induced difference absorption signals at eight pairs of wavelengths in the visible range of the spectrum between 505 and 570 nm. The first two wavelength pairs at 505 to 520 and 520 to 535 nm are dominated by the electrochromic shift as well as by the slow zeaxanthin to violaxanthin conversion (505 to 520 nm) and the scattering signal most likely arising from PsbS protonation (520 to 535 nm). The other wavelength pairs (540 to 545 nm, 545 to 550nm, 550 to 554 nm, 554 to 559 nm, 559 to 563nm, and 563 to 570nm) are mainly used for the measurements of the C550 pheophytin signal and of cytochrome signals. The ECS was deconvoluted from signals arising from zeaxanthin formation, scattering effects, the C550 signal, and from redox changes of the cytochromes *f*, b_6, and b_{559}, essentially as described by Klughammer et al. (1990). The deconvoluted transmission signals (ΔI/I) were then normalized to the chlorophyll content of the measured leaf section.

The maximum amplitude of the ECS (ECS_T) was used as a measure for the light-induced pmf across the thylakoid membrane. The measurements were performed at 20°C under CO_2-saturated conditions (2000 ppm). Leaves were illuminated for 10 min prior to each measurement to allow photosynthesis to reach steady state. ECS_T was determined after illuminating the leaves with saturating light (2100 μmol photons m^{-2} s^{-1}), which then was interrupted by a short interval of darkness (15 s), and the dark-interval relaxation kinetics of the ECS and of cyt-f (cyt-f) reduction were measured. Dark intervals (15 s) were sufficient for complete relaxation of the pmf. To obtain light saturation curves of the pmf, dark-interval relaxation kinetics after illumination at subsaturating light intensities between 200 and 2100 μmol photons m^{-2} s^{-1} were measured. pmf partitioning into ΔpH and $\Delta\Psi$ was resolved by analyzing the slowly relaxing phase of the ECS between 1 and 15 s of darkness as described by Takizawa et al. (2007).

To determine ATP synthase activity, the fast phase (between 0 and 500 ms after the end of actinic illumination) of the dark-interval relaxation kinetics measured at saturating light (2100 μmol photons m^{-2} s^{-1}) was fitted with a single exponential decay function. The reciprocal value of the halftime of the ECS decay, the thylakoid conductivity (gH^+), was used as a measure of ATP synthase activity because fast ECS decay is exclusively attributable to proton efflux through the ATP synthase (Cruz et al., 2001; Baker et al., 2007).

Thylakoid Membrane Isolation and Quantitation of Photosynthetic Complexes

Thylakoid membranes were isolated according to Schöttler et al. (2004). The contents of PSII and cyt-bf were determined from difference

absorption signals of cyt-b_{559} (PSII) and cyt-*f* and b_6 (cyt-bf). Thylakoids equivalent to 50 μg chlorophyll mL^{-1} were destacked in a low salt medium to improve the optical properties of the probe (Kirchhoff et al., 2002). All cytochromes were oxidized by the addition of 1 mM potassium ferricyanide (+III) and subsequently reduced by addition of 10 mM sodium ascorbate and dithionite, resulting in the reduction of cyt-*f* and the high-potential form of cyt-b_{559} (ascorbate-ferricyanide difference spectrum) and of cyt-b_6 and the low-potential form of cyt-b_{559}, respectively. At each redox potential, absorption spectra were measured between 575- and 540-nm wavelength with a V-550 spectrophotometer (Jasco) equipped with a head-on photomultiplier. The spectral bandwidth was 1 nm, and the scanning speed was 100 nm min^{-1}. Difference absorption spectra were deconvoluted using reference spectra and difference extinction coefficients as by Kirchhoff et al. (2002). PSII contents were calculated from the sum of the high- and low-potential difference absorption signals of cyt-b_{559} (Lamkemeyer et al., 2006).

The content of redox-active PSI was determined from light-induced difference absorption changes of P_{700}, the PSI reaction center chlorophyll-*a* special pair dimer. Isolated thylakoids equivalent to 50 μg chlorophyll mL^{-1} were solubilized with 0.2% (w/v) β-dodecylmaltoside in the presence of 100 μM paraquat as electron acceptor and of 10 mM sodium ascorbate as electron donor. P_{700} was oxidized by the application of a saturating light pulse (2000 μmol photons m^{-2} s^{-1} red light, 200-ms duration). Measurements were done using the Dual-PAM instrument (Heinz Walz) in its PC-P_{700} version (see below).

PC contents, relative to P_{700}, were determined by in vivo difference absorption spectroscopy in the far-red range of the spectrum and then recalculated based on the absolute P_{700} quantification in isolated thylakoids (see above). Light-induced absorption changes at 800-to 870-nm wavelength (where the contribution of P_{700} is predominant) and at 870- to 950-nm wavelength (predominantly arising from PC) were measured on preilluminated leaves with a fully activated Calvin cycle to avoid acceptor side limitation of PSI (Schöttler et al., 2007a). To determine the maximum difference absorption signals of PC and PSI, preilluminated leaves were transferred into darkness for a few seconds to fully reduce both components, and this was followed by 8 s of illumination with far-red light (715-nm wavelength) to selectively excite PSI. Then, a saturating pulse of red light was applied (635-nm wavelength, 5000 μmol photons m^{-2} s^{-1}, 200-ms duration), to completely oxidize PC and PSI and reduce the PSII side of the electron transport chain. At the end of the actinic light pulse, all light sources were switched off, and PC and PSI reduction kinetics were determined.

Chlorophyll-*a* Fluorescence

The 77K chlorophyll-*a* fluorescence emission was determined on freshly isolated thylakoids equivalent to 10 μg chlorophyll mL^{-1} using an F-6500 fluorometer (Jasco). The sample was excited at 430-nm wavelength (10-nm bandwidth). The emission spectra between 655 and 800 nm were recorded with a bandwidth of 1 nm. Chlorophyll-*a* fluorescence of intact leaves was measured at room temperature using a Dual-PAM-100 instrument (Heinz Walz). Light-response curves of linear electron flux and of nonphotochemical quenching as well as of the redox state of the PQ pool were recorded on intact leaves after 30 min of dark adaptation. The redox state of the PSII acceptor side was calculated from the qL parameter (Kramer et al., 2004), while qN was determined according to Krause and Weis (1991). Electron transport rates were corrected for leaf absorptance (see above).

Protein Gel Electrophoresis and Protein Gel Blots

Thylakoid proteins separated by SDS-PAGE (Perfect Blue twin gel system; Peqlab) were transferred to a polyvinylidene difluoride membrane (Hybond P) using a tank blotting system (Perfect Blue Web M; PeqLab). Specific polyclonal antibodies produced in rabbit against PsbD, PetA, PsaA, AtpA, and AtpB were purchased from AgriSera. As secondary antibody, an anti-rabbit IgG peroxidize conjugate was used (Sigma-Aldrich). Immunochemical detection was performed with the ECL system (GE Healthcare) according to the instructions of the manufacturer. Signal intensities of the x-ray films were quantified using the ImageQuant software (GE Healthcare) as described (Drechsel and Bock, 2010).

Accession Numbers

Sequence data from this article can be found in the GenBank/EMBL data libraries under the following accession numbers: *N. tabacum* chloroplast genome DNA containing the annotated genes of *accD*, *rbcL*, *atpB*, and *atpE* (Z00044.2); *aadA* selectable marker gene for chloroplast transformation (AJ312391.1), and *N. tabacum atpC* EST (X63606.1).

ACKNOWLEDGMENTS

We thank Stephanie Ruf and Yvonne Weber for chloroplast transformation, selection, and plant regeneration and Britta Hausmann for plant cultivation. This project was supported by a grant from the Deutsche Forschungsgemeinschaft to M.A.S. and R.B. (SFB 429, Project A12).

Received August 27, 2010; revised December 13, 2010; accepted January 5, 2011; published January 28, 2011.

REFERENCES

Anderson, J.M. (1992). Cytochrome b6f complex: Dynamic molecular organization, function and acclimation. Photosynth. Res. **34:** 341–357.

Anderson, J.M., Chow, W.S., and Goodchild, D.J. (1988). Thylakoid membrane organisation in sun/shade acclimation. Aust. J. Plant Physiol. **15:** 11–26.

Aro, E.M., Suorsa, M., Rokka, A., Allahverdiyeva, Y., Paakkarinen, V., Saleem, A., Battchikova, N., and Rintamäki, E. (2005). Dynamics of photosystem II: A proteomic approach to thylakoid protein complexes. J. Exp. Bot. **56:** 347–356.

Bailey, S., Walters, R.G., Jansson, S., and Horton, P. (2001). Acclimation of *Arabidopsis thaliana* to the light environment: The existence of separate low light and high light responses. Planta **213:** 794–801.

Baker, N.R., Harbinson, J., and Kramer, D.M. (2007). Determining the limitations and regulation of photosynthetic energy transduction in leaves. Plant Cell Environ. **30:** 1107–1125.

Barkan, A. (1998). Approaches to investigating nuclear genes that function in chloroplast biogenesis in land plants. Methods Enzymol. **297:** 38–57.

Bock, R. (2001). Transgenic plastids in basic research and plant biotechnology. J. Mol. Biol. **312:** 425–438.

Boeck, R., and Kolakofsky, D. (1994). Positions +5 and +6 can be major determinants of the efficiency of non-AUG initiation codons for protein synthesis. EMBO J. **13:** 3608–3617.

Bosco, C.D., Lezhneva, L., Biehl, A., Leister, D., Strotmann, H., Wanner, G., and Meurer, J. (2004). Inactivation of the chloroplast ATP synthase gamma subunit results in high non-photochemical fluorescence quenching and altered nuclear gene expression in *Arabidopsis thaliana.* J. Biol. Chem. **279:** 1060–1069.

Bunney, T.D., van Walraven, H.S., and de Boer, A.H. (2001). 14-3-3 protein is a regulator of the mitochondrial and chloroplast ATP synthase. Proc. Natl. Acad. Sci. USA **98:** 4249–4254.

Burkey, K.O. (1993). Effect of growth irradiance on plastocyanin levels in barley. Photosynth. Res. **36:** 103–110.

Burkey, K.O. (1994). Genetic variation of electron transport in barley: Identification of plastocyanin as potential limiting factor. Plant Sci. **98:** 177–187.

Chen, L.J., Rogers, S.A., Bennett, D.C., Hu, M.C., and Orozco, E.M., Jr. (1990). An in vitro transcription termination system to analyze chloroplast promoters: Identification of multiple promoters for the spinach atpB gene. Curr. Genet. **17:** 55–64.

Cruz, J.A., Sacksteder, C.A., Kanazawa, A., and Kramer, D.M. (2001). Contribution of electric field (Delta psi) to steady-state transthylakoid proton motive force (pmf) in vitro and in vivo. control of pmf parsing into Delta psi and Delta pH by ionic strength. Biochemistry **40:** 1226–1237.

del Riego, G., Casano, L.M., Martín, M., and Sabater, B. (2006). Multiple phosphorylation sites in the β subunit of thylakoid ATP synthase. Photosynth. Res. **89:** 11–18.

Doyle, J.J., and Doyle, J.L. (1990). Isolation of plant DNA from fresh tissue. Focus **12:** 13–15.

Drapier, D., Rimbault, B., Vallon, O., Wollman, F.A., and Choquet, Y. (2007). Intertwined translational regulations set uneven stoichiometry of chloroplast ATP synthase subunits. EMBO J. **26:** 3581–3591.

Drechsel, O., and Bock, R. (2011). Selection of Shine-Dalgarno sequences in plastids. Nucleic Acids Res., in press.

Eberhard, S., Drapier, D., and Wollman, F.A. (2002). Searching limiting steps in the expression of chloroplast-encoded proteins: Relations between gene copy number, transcription, transcript abundance and translation rate in the chloroplast of *Chlamydomonas reinhardtii*. Plant J. **31:** 149–160.

Evans, J.R. (1988). Acclimation by the thylakoid membranes to growth irradiance and the partitioning of nitrogen between soluble and thylakoid proteins. Aust. J. Plant Physiol. **15:** 93–106.

Fernie, A.R., Carrari, F., and Sweetlove, L.J. (2004). Respiratory metabolism: Glycolysis, the TCA cycle and mitochondrial electron transport. Curr. Opin. Plant Biol. **7:** 254–261.

Gross, E.L., Pan, B., Li, B., and Brown, L. (1994). Stability of plastocyanin to acid pH. Biophys. J. **66:** 272.

Hirose, T., Ideue, T., Wakasugi, T., and Sugiura, M. (1999). The chloroplast infA gene with a functional UUG initiation codon. FEBS Lett. **445:** 169–172.

Hirose, T., and Sugiura, M. (2004). Multiple elements required for translation of plastid *atpB* mRNA lacking the Shine-Dalgarno sequence. Nucleic Acids Res. **32:** 3503–3510.

Hope, A.B. (2000). Electron transfers amongst cytochrome f, plastocyanin and photosystem I: Kinetics and mechanisms. Biochim. Biophys. Acta **1456:** 5–26.

Kanazawa, A., and Kramer, D.M. (2002). In vivo modulation of nonphotochemical exciton quenching (NPQ) by regulation of the chloroplast ATP synthase. Proc. Natl. Acad. Sci. USA **99:** 12789–12794.

Kiirats, O., Cruz, J.A., Edwards, G.E., and Kramer, D.M. (2009). Feedback limitation of photosynthesis at high CO_2 acts by modulating the activity of the chloroplast ATP synthase. Funct. Plant Biol. **36:** 893–901.

Kim, C., Meskauskiene, R., Apel, K., and Laloi, C. (2008). No single way to understand singlet oxygen signalling in plants. EMBO Rep. **9:** 435–439.

Kirchhoff, H., Horstmann, S., and Weis, E. (2000). Control of the photosynthetic electron transport by PQ diffusion microdomains in thylakoids of higher plants. Biochim. Biophys. Acta **1459:** 148–168.

Kirchhoff, H., Mukherjee, U., and Galla, H.J. (2002). Molecular architecture of the thylakoid membrane: Lipid diffusion space for plastoquinone. Biochemistry **41:** 4872–4882.

Klughammer, C., Kolbowski, J., and Schreiber, U. (1990). LED array spectrophotometer for measurement of time resolved difference spectra in the 530–600 nm wavelength region. Photosynth. Res. **25:** 317–327.

Kohzuma, K., Cruz, J.A., Akashi, K., Hoshiyasu, S., Munekage, Y.N., Yokota, A., and Kramer, D.M. (2009). The long-term responses of the photosynthetic proton circuit to drought. Plant Cell Environ. **32:** 209–219.

Kooter, J.M., Matzke, M.A., and Meyer, P. (1999). Listening to the silent genes: Transgene silencing, gene regulation and pathogen control. Trends Plant Sci. **4:** 340–347.

Kramer, D.M., Cruz, J.A., and Kanazawa, A. (2003). Balancing the central roles of the thylakoid proton gradient. Trends Plant Sci. **8:** 27–32.

Kramer, D.M., Johnson, G., Kiirats, O., and Edwards, G.E. (2004). New fluorescence parameters for the determination of q(a) redox state and excitation energy fluxes. Photosynth. Res. **79:** 209–218.

Kramer, D.M., Sacksteder, C.A., and Cruz, J. (1999). How acidic is the lumen? Photosynth. Res. **60:** 151–163.

Krause, G.H., and Weis, E. (1991). Chlorophyll-a fluorescence and photosynthesis: The basics. Annu. Rev. Plant Physiol. Plant Mol. Biol. **42:** 313–349.

Krieger, A., and Weis, E. (1993). The role of calcium in the pH-dependent control of photosystem II. Photosynth. Res. **37:** 117–130.

Lamkemeyer, P., et al. (2006). Peroxiredoxin Q of *Arabidopsis thaliana* is attached to the thylakoids and functions in context of photosynthesis. Plant J. **45:** 968–981.

Lein, W., Usadel, B., Stitt, M., Reindl, A., Ehrhardt, T., Sonnewald, U., and Börnke, F. (2008). Large-scale phenotyping of transgenic tobacco plants (*Nicotiana tabacum*) to identify essential leaf functions. Plant Biotechnol. J. **6:** 246–263.

Majeran, W., Wollman, F.-A., and Vallon, O. (2000). Evidence for a role of ClpP in the degradation of the chloroplast cytochrome b(6)f complex. Plant Cell **12:** 137–150.

Oswald, O., Martin, T., Dominy, P.J., and Graham, I.A. (2001). Plastid redox state and sugars: interactive regulators of nuclear-encoded photosynthetic gene expression. Proc. Natl. Acad. Sci. USA **98:** 2047–2052.

Pfannschmidt, T., Bräutigam, K., Wagner, R., Dietzel, L., Schröter, Y., Steiner, S., and Nykytenko, A. (2009). Potential regulation of gene expression in photosynthetic cells by redox and energy state: Approaches towards better understanding. Ann. Bot. (Lond.) **103:** 599–607.

Pfannschmidt, T., Nilsson, A., and Allen, J.F. (1999). Photosynthetic control of chloroplast gene expression. Nature **397:** 625–628.

Pogson, B.J., Woo, N.S., Förster, B., and Small, I.D. (2008). Plastid signalling to the nucleus and beyond. Trends Plant Sci. **13:** 602–609.

Porra, R.J., Thompson, W.A., and Kriedermann, P.E. (1989). Determination of accurate extinction coefficient and simultaneous equations for essaying chlorophylls a and b extracted with four different solvents: Verification of the concentration of chlorophyll standards by atomic absorption spectroscopy. Biochim. Biophys. Acta **975:** 384–394.

Price, G.D., von Caemmerer, S., Evans, J.R., Siebke, K., Anderson, J.M., and Badger, M.R. (1998). Photosynthesis is strongly reduced by antisense suppression of chloroplastic cytochrome bf complex in transgenic tobacco. Aust. J. Plant Physiol. **25:** 445–452.

Price, G.D., Yu, J.W., von Caemmerer, S., Evans, J.R., Chow, W.S., Anderson, J.M., Hurry, V., and Badger, M.R. (1995). Chloroplast cytochrome b_6/f and ATP synthase complexes in tobacco: Transformation with antisense RNA against nuclear-encoded transcripts for the Rieske FeS and ATPδ polypeptides. Aust. J. Plant Physiol. **22:** 285–297.

Reiland, S., Messerli, G., Baerenfaller, K., Gerrits, B., Endler, A., Grossmann, J., Gruissem, W., and Baginsky, S. (2009). Large-scale *Arabidopsis* phosphoproteome profiling reveals novel chloroplast kinase substrates and phosphorylation networks. Plant Physiol. **150:** 889–903.

Rogalski, M., Schöttler, M.A., Thiele, W., Schulze, W.X., and Bock, R. (2008). Rpl33, a nonessential plastid-encoded ribosomal protein in tobacco, is required under cold stress conditions. Plant Cell **20:** 2221–2237.

Rosahl, S., Schell, J., and Willmitzer, L. (1987). Expression of a tuber-specific storage protein in transgenic tobacco plants: demonstration of an esterase activity. EMBO J. **6:** 1155–1159.

Schöttler, M.A., Flügel, C., Thiele, W., and Bock, R. (2007b). Knock-out of the plastid-encoded PetL subunit results in reduced stability and accelerated leaf age-dependent loss of the cytochrome b6f complex. J. Biol. Chem. **282:** 976–985.

Schöttler, M.A., Flügel, C., Thiele, W., Stegemann, S., and Bock, R. (2007a). The plastome-encoded PsaJ subunit is required for efficient Photosystem I excitation, but not for plastocyanin oxidation in tobacco. Biochem. J. **403:** 251–260.

Schöttler, M.A., Kirchhoff, H., and Weis, E. (2004). The role of plastocyanin in the adjustment of the photosynthetic electron transport to the carbon metabolism in tobacco. Plant Physiol. **136:** 4265–4274.

Schwassmann, H.J., Rexroth, S., Seelert, H., and Dencher, N.A. (2007). Metabolism controls dimerization of the chloroplast FoF1 ATP synthase in *Chlamydomonas reinhardtii*. FEBS Lett. **581:** 1391–1396.

Sharkey, T.D., and Vanderveer, P.J. (1989). Stromal phosphate concentration is low during feedback limited photosynthesis. Plant Physiol. **91:** 679–684.

Sugiura, M., Hirose, T., and Sugita, M. (1998). Evolution and mechanism of translation in chloroplasts. Annu. Rev. Genet. **32:** 437–459.

Svab, Z., and Maliga, P. (1993). High-frequency plastid transformation in tobacco by selection for a chimeric aadA gene. Proc. Natl. Acad. Sci. USA **90:** 913–917.

Szabó, I., Bergantino, E., and Giacometti, G.M. (2005). Light and oxygenic photosynthesis: Energy dissipation as a protection mechanism against photo-oxidation. EMBO Rep. **6:** 629–634.

Takizawa, K., Cruz, J.A., Kanazawa, A., and Kramer, D.M. (2007). The thylakoid proton motive force in vivo. Quantitative, non-invasive probes, energetics, and regulatory consequences of light-induced pmf. Biochim. Biophys. Acta **1767:** 1233–1244.

Takizawa, K., Kanazawa, A., and Kramer, D.M. (2008). Depletion of stromal P(i) induces high 'energy-dependent' antenna exciton quenching (q(E)) by decreasing proton conductivity at CF(O)-CF(1) ATP synthase. Plant Cell Environ. **31:** 235–243.

Tezara, W., Mitchell, V.J., Driscoll, S.D., and Lawlor, D.W. (1999). Water stress inhibits plant photosynthesis by decreasing coupling factor and ATP. Nature **401:** 914–917.

Wu, G., and Ort, D.R. (2008). Mutation in the cysteine bridge domain of the gamma-subunit affects light regulation of the ATP synthase but not photosynthesis or growth in Arabidopsis. Photosynth. Res. **97:** 185–193.

Wu, G., Ortiz-Flores, G., Ortiz-Lopez, A., and Ort, D.R. (2007). A point mutation in atpC1 raises the redox potential of the *Arabidopsis* chloroplast ATP synthase gamma-subunit regulatory disulfide above the range of thioredoxin modulation. J. Biol. Chem. **282:** 36782–36789.